ABSTRACT

Title of Document:	PROBING BIOMECHANICAL PROPERTIES OF SINGLE MOLECULE SYSTEMS USING OPTICAL TWEEZERS
	Adam P. Karcz, Master of Science, 2010
Directed By:	Assistant Professor/Advisor, Joonil Seog, Department of Materials Science and Engineering

Single molecule techniques have provided novel mechanistic insights on biological processes such as protein folding, transcription, and motor protein movement. Using single molecule methods, the distribution of individual molecular behavior is directly measured, which cannot be obtained using conventional bulk approaches. In this study, custom-built optical tweezers with sub-pN force resolution were used to probe the dynamic behavior of DNA:cationic carrier complex. Two histidine-lysine (HK) based polymers (H_3K4b vs H_3KG4b) were used to compare their condensation behaviors at the single molecular level. The difference between the two HK polymers at the single molecule level may have a significant implication as to why H_3KG4b shows much higher gene delivery efficiency than H_3K4b. The optical tweezers were also used to probe the unfolding processes of a fragment of F4 RNA. This can be used to characterize secondary structures in RNA, such as hairpins and pseudoknots.

PROBING BIOMECHANICAL PROPERTIES OF SINGLE MOLECULE SYSTEMS
USING OPTICAL TWEEZERS

By

Adam P. Karcz

Thesis submitted to the Faculty of the Graduate School of the
University of Maryland, College Park, in partial fulfillment
of the requirements for the degree of
Master of Science
2011

Advisory Committee:
Assistant Professor Joonil Seog, Chair
Professor Lourdes Salamanca-Riba
Professor Manfred Wuttig

Acknowledgments

Table of Contents

List of Tables

List of Figures

List of Abbreviations and Acronyms

DNA   deoxyribonucleic acid

RNA   ribonucleic acid

OT   optical tweezers

PD   photodetector

PSD   position sensitive detector

LED   light emitting diode

PBS   polarizing beam splitter (when referring to optics)
                phosphate buffered saline (when referring to buffer)

Piezo   piezoelectric actuator

ADC   analog to digital converter

CCD   charge coupled device

OBJ   objective

PCR   polymer chain reaction

bp   basepair

nt   nucleotide

Chapter 1: Introduction

The main focus of these single molecule experiments lies in comparing gene carriers. Gene delivery has been studied as a promising treatment for hereditary diseases for a few decades with a limited success. Several non-viral carriers for nucleic acids have been developed as *in vitro* and *in vivo* transfection agents.[1, 2] The cationic carriers package DNA into a compact and slightly positively charged nanoscale complex.[3-5] Most non-viral carriers depend on endocytosis to be imported inside cells; hence various endosomal escape strategies have been developed to increase transfection efficiency.[6, 7] However, the DNA unpackaging process, which is considered as one of the critical steps to enhance the efficiency of gene delivery, has not yet been studied in detail. The dynamic mechanical properties of the nanoplex are likely to impact DNA unpackaging process directly, hence the transfection efficiency.

The current bottlenecks in developing an efficient gene carrier is not the lack of synthesizing novel gene carriers, but the limited understanding of the molecular level processes such as disintegration of the DNA:carrier complex inside the endosome. Furthermore, the correlation between the structures of cationic carriers and their transfection efficiency is very poorly understood.

Understanding the dynamic properties of DNA complex is crucial to enhance efficiency of gene delivery. Specifically the regulation of mechanical behaviors of DNA complex under physiological conditions can provide a significant insight on how to design a carrier molecule with optimum efficacy. In this study, the mechanical condensation and decondensation of DNA:peptide complex was directly investigated at the single molecule level using custom built optical tweezers. Two histidine-lysine (HK)

based peptides, H$_3$K4b and H$_3$KG4b, with vastly different transfection efficiencies were used. During stretching andrelaxation cycles of DNA: peptide complex, partial decondensation and recondensation were observed with hysteretic behavior. The amount of the hysteresis decreased as ionic strength increased, confirming that electrostatic interaction is the major driving force of the DNA:HK complex formation. The dramatic increase in decondensation length of the complex was observed when pH was lowered to mimic endosomal conditions. After a sudden expansion, the decondensation length of H$_3$K4b decreased after several minutes whereas H$_3$KG4b maintained a nearly fully decondensed length for an extended period of time. The remarkable difference between two HK polymers at the single molecule level may have a significant implication to the striking differences in their transfection efficiency measured in vitro.

Studying of RNA unfolding has also been made possible with optical tweezers [8-11]. However, it has not been yet attempted to use optical tweezers as a tool to characterize structures of RNA given an unknown RNA system. Preliminary results for such a method are presented by looking at F1 RNA to characterize its different structural elements, such as hairpins and pseudoknots.

Chapter 2: Optical Tweezers Principles and Design

Optical tweezers design was done at the University of California, Berkeley, where I worked with Steven B. Smith of the Carlos Bustamante lab, working on the miniTweezers instrument. More information of the instrument can be found at http://tweezerslab.unipr.it; however, all information regarding the instrument will be discussed below.

2.1: Optical Tweezers Principles

2.1.1: Force Measurement

Optical tweezers are capable of trapping small, dielectric particles because of the gradiant caused by the pinching of laser light to a small spot through the use of focusing lenses. This gradient causes the particles to be attracted to the point of largest gradient, the laser focus. With this, one can imagine the optical trap as a Hookean spring with spring constant, k, such that $F=kx$, and the force can be calculate from displacement. The spring constant could be calculated from the equipartition theorem as $\frac{1}{2}k<x^2>=\frac{1}{2}k_BT$; however, this would require accurate tracking of displacement of the trapped particle and recalibration for different trapped bead sizes, so other methods are used. Because a photon carries a linear momentum, $P = \hbar/\lambda$, where $\hbar$ is Planck's constant and λ is the wavelength of the photon, in its direction of motion, some of the photons can be absorbed or scattered by the particle, and cause it to drift slightly from the laser focus. A light beam (a collection of photons) creates a force which is absorbed by object, $F = dP/dt = nW/c$, where n is the refractive index of the medium ($n_{air} = 1.0$, $n_{water} = 1.33$), W is the power of the light beam, and c is the speed of light. This comes from the integration of light momentum flux, which is given by[12] $d(dP/dt) = (n/c)SdA$, where S is Poynting's

vector, and A is the area. Furthermore, through the use of the Abbe sine condition and energy conservation[12], the force can be simplified to

$$F_x = \frac{D_x R_D}{c \Psi R_L} \qquad F_y = \frac{D_y R_D}{c \Psi R_L}$$

where R_D is the effective radius of the detector, R_L is the focal length of the lens which focuses the light onto the detector, and Ψ is a sensitivity of the detectors in watts/count. D_x and D_y are detector signals, given by

$$D_x = \Psi \iint E(x,y)(x/R_D)dA$$

$$D_y = \Psi \iint E(x,y)(y/R_D)dA$$

where E is the irradiance in watts/m^2. Thus, changes in the detector signal can be correlated to the forces which cause beam deflection.
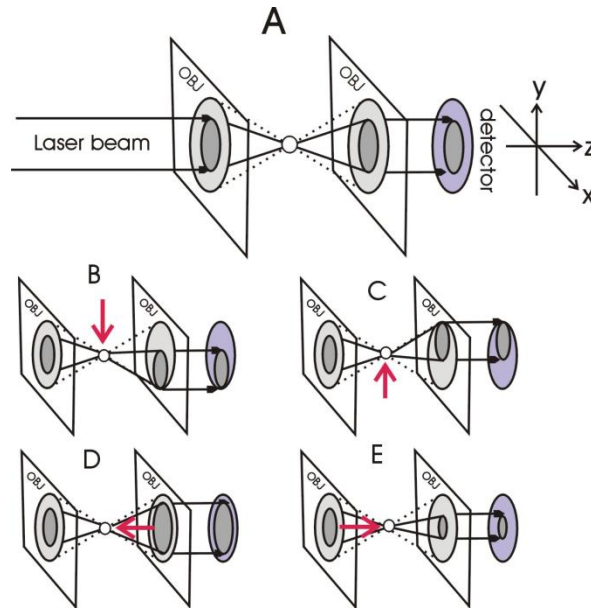
Figure 1. (A) The optical trap is shown in its undisturbed configuration. (B and C) Displacement in the bead due to outside force causes deflection in the laser beam. This can be used to measure forces in X and Y directions. (D and E) Z-force can be measure due to the changes in beam width when the particle is displace longitudinally. Image is courtesy of Steven B. Smith.

The optical tweezers instrument used here has dual counter-propagating beams, which serve to cancel any scattering or absorption effects that would otherwise displace the trapped particle. As such, it is possible to measure the force acting in the Z-axis, which is described later in the calibration section (3.8).

2.1.2: Resolution

One question that always comes to mind when dealing with single molecule experiments is, "What is the resolution of your instrument?" The detectors themselves can provide data at a 1 kHz rate, but distance and force resolution are also important. Shown in Fig. 2 is a "hopping test." A hopping test causes the two counter-propagating
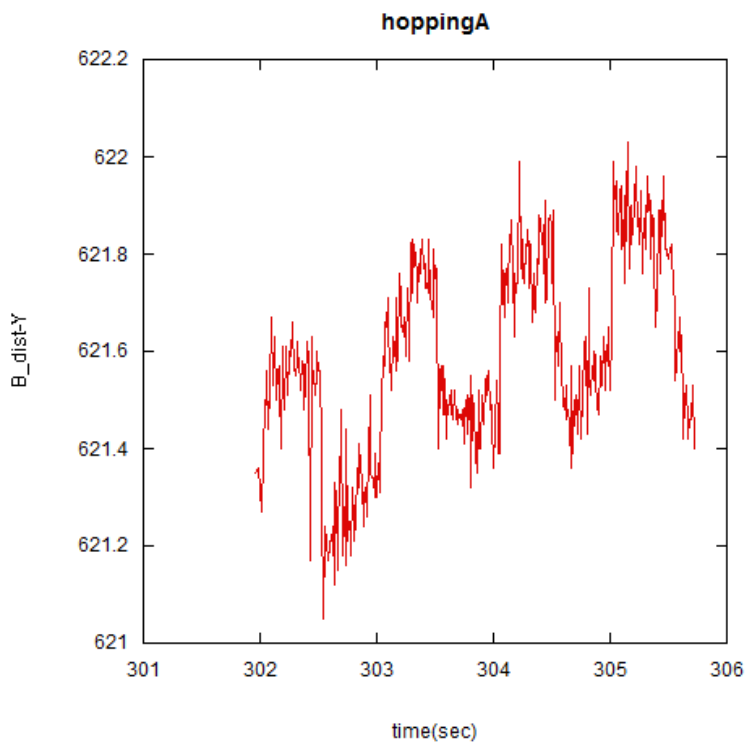
Figure 2. Hopping test showing the distance resolution of the optical tweezers.

lasers to move in opposite direction. The distance is varied a set amount (0.33 nm in Fig. 2), changing once a second which causes step-like behavior. The signal-to-noise ratio (ratio of step size to standard error of a step) was calculated to be about 4.4. Since the smallest unit of displacement that the piezoelectric actuator can move is 0.15 nm, we can find the distance resolution to be

$$Resolution = \frac{X_{min}\sqrt{t}}{SNR}$$

where X_{min} is the minimum displacement, SNR is the signal-to-noise ratio, and t is the length of time of the step. Hence, the resolution is 0.34 Å/Hz$^{1/2}$. By using a variation of the hopping test where the force is being being changed in equal and opposite amounts for the two lasers (total change in force is zero), we can perform a stiffness test. Over several experiments, the stiffness was found to be 0.060 pN/nm. Therefore, the force resolution of this instrument is 2 fN/ Hz$^{1/2}$.

2.2: Optical Tweezers Design

First, a description of each of the components of this optical tweezers instrument, which is named the miniTweezers for its compactness, will be explained. Then, a full description of the path that the laser beams travel will be provided.
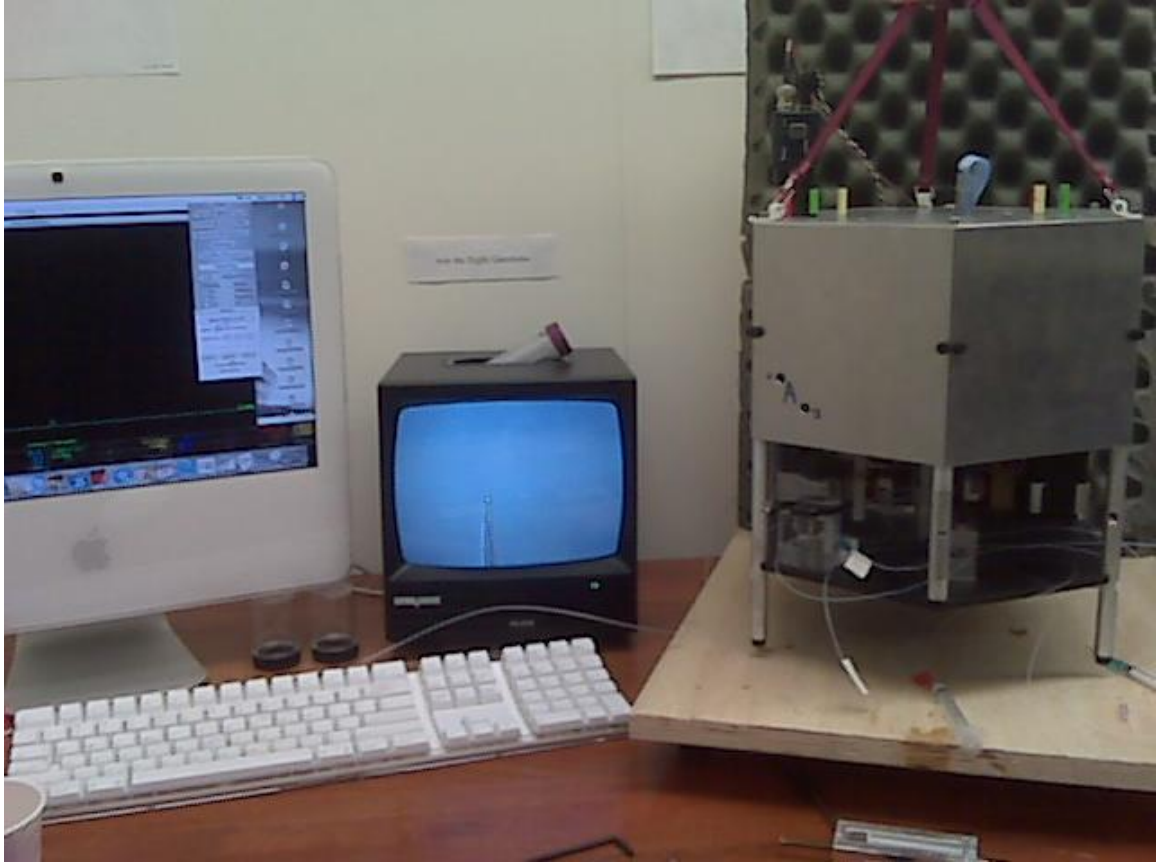
Figure 3. The optical tweezers instrument (shown on right) is pictured with CCD screen (middle) and host computer (left).

2.2.1: Instrument Head

Framework – The housing for the optical parts is made from machined aluminum. Most of the instrument is made from either aluminum or brass, which have similar thermal expansion coefficients.

Lasers – Two of these are attached to the lid. They provide laser light of a wavelength of 845 nm and up to 150 mW of continuous laser power

Motorized stage – This component controls the movement of the micro-fluidics chamber so that the sample can be manipulated in three dimensions. This is especially important for trapping polystyrene beads.

Fiber Wiggler – This assembly controls the position of the fiber optic end. A piezoelectric actuator moves this part in lateral directions with respect to direction of the light beam.

Force Detector – This is a detector system which uses a position sensitive detector (PSD) to measure changes in force in X and Y directions and a separate photodector (PD) to measure changes in Z-force via a "Bullseye" filter.

Position Detector – This position sensitive detector tracks the position of the laser beam in X and Y directions. Displacements at the fiber optic end are recorded with it.

LED Light Source – The purpose of this part is to provide background light for imaging the sample plane onto the CCD camera.

Relay Lens Assembly – A pair of lenses help to overfill the force detectors so that all the light can be accurately convert offsets in overall photon position into force offset.

Position Detector Upper Periscope – Uses mirrors to relay light from the Lower Optical Train to the position detector.

Position Detector Adjustment Mirror – This mirror can be adjusted at angles to change the position of the beam onto the detector.

Lower Optics Train – This combination of parts lies underneath the instrument head.

> Prism Box – A container for two polarizing beam splitters (PBS) and two right angle corner reflectors, its purpose is to reflect different polarizations of light through separate optical paths.

> Position Detector Lower Periscope – Similar in function to the upper periscope. It relays light from below the instrument back inside.

> Optical Rail and Objective Sliding Mount – This holds the quarter wave plates and objectives in place. The Prism Box also attaches to it.

> Beam Block – Black delrin blocks are used to prevent light from escaping the prism boxes.

Microchamber – This is the sample chamber for experiments (shown below). It has three channels going across the top, middle, and bottom. Tubing is connected to each side of the microchamber for injecting buffers or samples from the side holes. The middle channel is where the experiments are actually performed. It has the pipette tip located at its center, where a small bead can be trapped by suction. The optical trap will hold a second bead which can be used for stretching molecules, using the focused laser beam from the objectives.
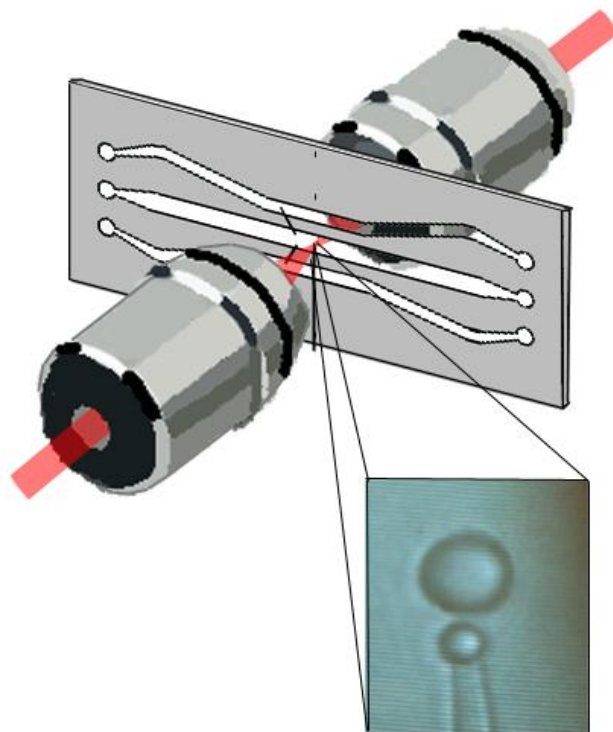
Figure 4. A drawing of the microchamber is shown with objectives that focus the laser light. The inset shows the CCD image of the bead attached to the pipette (lower bead) and the bead that is trapped by the lasers (upper bead).

2.2.2: Laser Power Supply

This unit supplies variable laser power for optical trapping using a simple dial. The laser

cooling is controlled using this unit, as well. There is a knob to changing the display

settings, which is described later.

2.2.3: Controller Power Supply

The controller power supply is responsible for all electronic communications between the

instrument and the computer. Three different power supplies are able to power different

parts of the optical tweezers, such as the motors and piezos. There are four types of

printed circuit boards which are processing commands for separate functions. Here, they

are listed in order from top to bottom as they appear on the power supply.

Main control board – This board communicates directly with the computer through USB.
It sends commands to all other boards. If there are any freeze-ups in the software, it can
usually be fixed by pressing the reset buttons on this board.

Piezo control board – This board controls the power (up to 150 V) being supplied to the
piezoelectric actuator. This, in effect, controls the laser spot position.

Motor control board – This board controls the movement of the motors, which
manipulate the position of the microchamber. This can be used to find beads to trap with
the optical tweezers. There is also a reset button on this board to reset the (0, 0, 0)
position in X, Y, and Z directions.

ADC control board – This board communicates with the different detectors in the optical
tweezers. Signals from the detectors are processed and sent to the main control board,
where they are further directed to the computer.

2.3: Laser Light Path

Laser light emits from an optical fiber in the "fiber wiggler," an assembly which

controls movement of the laser at the fiber end, and, hence, the laser focal position. Upon

exiting the optical fiber, the laser is split 95/5 by a pellicle. This pellicle reflects 5% of

the light towards a position sensitive detector via a "light lever" system. A small focusing

lens is used to image the focal point onto this detector. A series of mirrors within the

instrument reflect the light to minimize the space requirement for beam redirection. There

are three adjustment rods which turn screws on a kinematic bracket which acts as the

base for steering one of these mirrors so that the laser beam can focus at the center of the

detector. One rod controls x-axis movement, one controls y-axis
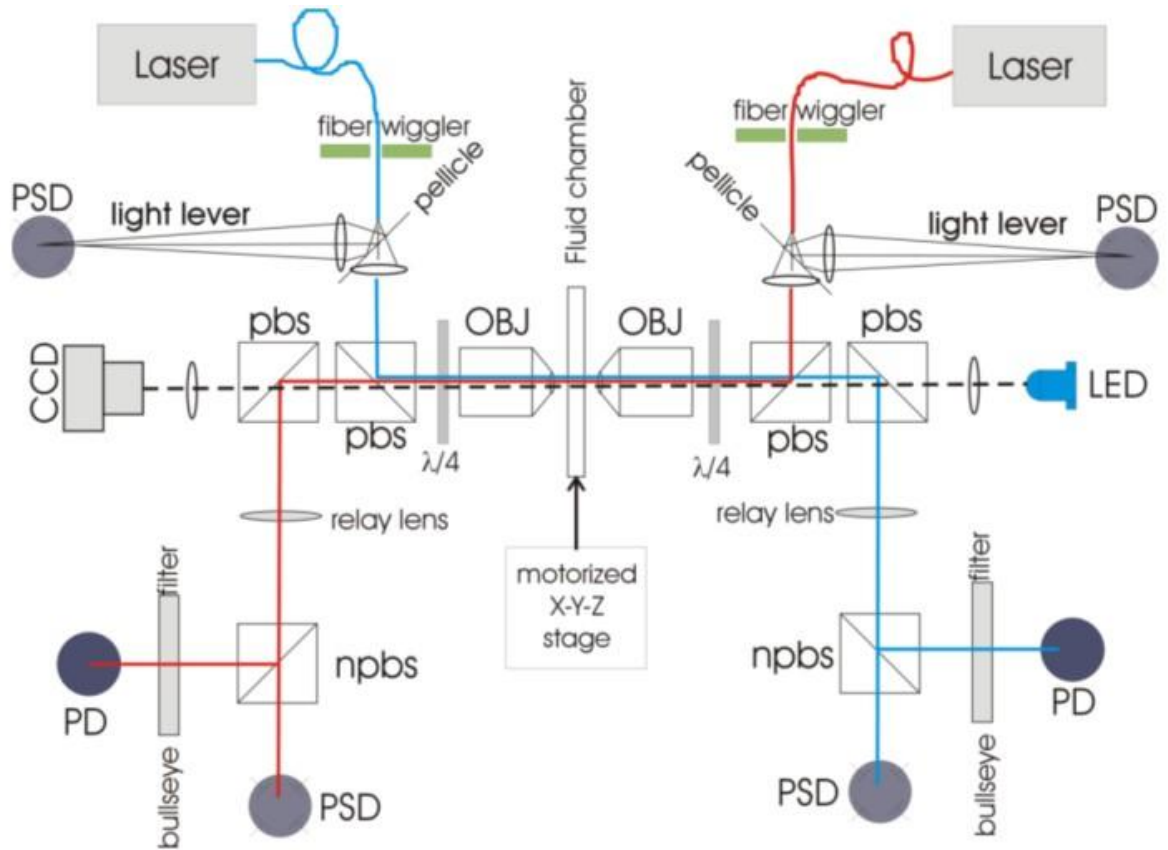
Figure 5. Schematic of the laser light path. Since there are two lasers, they are shown as different colors, red and blue. Image developed by Steven B. Smith (2009).

movement, and a third controls the corner of these two. The corner adjustment is meant to keep the two axes moving an equal forward or backward distance - this mimics z-axis movement. Additionally, there are piezoelectric actuators (piezos) which move the fiber end via a host program by as small as 0.1 nm displacements in X and Y axis. These piezos are in the fiber wiggler assembly.

The rest of the light is collimated by a lens. The beam then reaches a polarizing beam splitter which reflects S-polarized light and transmits P-polarized light. (In the case of Laser A, there is a retro-reflector which reflects the beam back up to the polarizing beam splitter. As a result, it becomes reflected at the beam splitter again and enters into a

second beam splitter which is oriented to transmit S-polarized light. This leads to the beam being imaged on a CCD camera. For Laser B, the beam continues straight into the CCD camera using a single polarizing beam splitter.) The S-polarized light which was reflected off the first beam splitter then reaches a quarter wave-plate which makes the light circularly polarized. It goes into an objective lens where it becomes focused in the sample plane. The sample plane is inside a micro-fluidics chamber where samples and trapped particles can be controlled. Then, the beam becomes collimated again after entering into an identical objective lens. The outgoing light reaches another quarter wave plate which makes the light P-polarized. There is another set of reflecting optics oriented in the same way as the previous set. The beam transmits through the first beam-splitter but is reflected off the second one. This light goes through a pair of relay lenses which are positioned to overfill the beam onto two detectors. A non-polarizing beam splitter makes 50% of light go to each detector. Half of it is directed to a position sensitive detector which records the force in X and Y directions. The other half records Z-force through the use of a "bullseye" filter which creates a hemispherical distribution of light onto a photodiode. Since the hemisphere filters more light at the extremities and filters least at the center, light that is more focused (converging) will provide a larger signal than light that is diverging. Since displacement along the Z-axis will cause the beam to diverge when in the negative Z-direction, the signal will be weaker on the detector. Likewise, the opposite will happen when there is displacement in the positive Z-direction. As such, the force change can be correlated to these changes in signal.

Chapter 3: Calibration of the Optical Tweezers

This section describes the calibration of the instrument while working in collaboration with Steven B. Smith at the University of California at Berkeley. Similar information can be found at the website for the system, *http://tweezerslab.unipr.it*.

3.1: Temperature Calibration

Using a thermometer, the temperature from inside the optical tweezers is taken. In the host program, the window for the oscilloscopes should be set to display A_Temp and B_Temp, lines which show the temperature of traps A and B, respectively. Centering can be enabled by pressing the C button to track the changes in temperature. It may be necessary to zoom into the signal with the Z button to rescale the Y axis. The readings should be close to the thermometer temperature. If they are not, it can be changed in the "ltCalibration" file by editing the temperature fudge factors.

3.2: Force Calibration

There are two ways to calibrate the force sensors. One method is by using a fluid drag (Stokes' law) test while the second is by using the known properties of light momentum. It is good to use both methods and compare results. If the tests agree with each other, it confirms the proper operation of the force detectors and strongly suggests that calibration will be immune to changes in bead size, bead composition, buffer composition, laser power, and focal quality. The Stokes' test only checks the combined force from two traps whereas the light momentum method gives individual force

calibration factors for the two traps A and B. However, the light momentum method does need both additional equipment and effort. There is a third test which can be done later, as confirmation, to check the overstretching force of a known sequence of dsDNA in a buffer of known salt concentration. This further affirms correct calibration of the optical tweezers.

3.2.1: Stokes' Law Calibration

First, fill the chamber with distilled water, which has a known viscosity versus temperature. The drag test force, F, will be proportional to the fluid viscosity, η, the velocity of movement, v, and the bead radius, r, according to Stokes' law:

$$F = 6\pi\eta vr.$$

Zero the PSDs with an empty trap and note the Iris/Sum ratios for both beams with an empty trap. Next, inject some polystyrene beads around 2 μm in diameter. It is necessary to know the bead size by some independent means, such as the manufacturer's specifications or a photograph of many beads from the distribution by using a calibrated electron microscope (SEM or TEM). Then, trap a bead in the counter-propagating beam foci. The beam deflections in the PSD window should deviate by equal and opposite amounts, indicating some beam misalignment. Enable Auto-Align, and the beam deflections in the PSD window should travel together to become near zero. Note the new Iris/Sum ratios, because if these ratios are higher than previously with an empty trap, then it will be necessary to adjust the inter-focal distance by turning the worm gear clockwise (CW) on the Objective Slider Mount (using a 5/64" hex driver). If these ratios were lower than with an empty trap, then turn the worm gear CCW. Stop when the current average of

the Iris/Sum readings agrees with the previous (empty) average within a 1% allowable

error. Turn Auto-Align off. Then select "Stokes Test" from "Tools" in the top menu. On

the new window, there are three spots that bounce up and down due to thermal

fluctuations: x-force is green, y-force is yellow, and z-force is blue. Press the button

"ZeroForce," and the three spots will become evenly spaced. Press "Move Motors XYZ"

which allows movement of the fluid chamber with the mouse. Adjust the Motor Speed

slider to the right to give maximum velocity with the mouse. These spots will form

scatter patterns with a slope. Forces are plotted vertically, and motor velocities are plotted

horizontally. The slope of the plots corresponds to the viscous drag coefficient of the

bead. Freeze the pattern with the *F* key. Then, rotate the pattern with the *Q* and *E* keys

until the patterns appear most horizontal. The apparent bead size (from Stokes' law) is

displayed in the lower left corner of the test window. If the bead size matches the
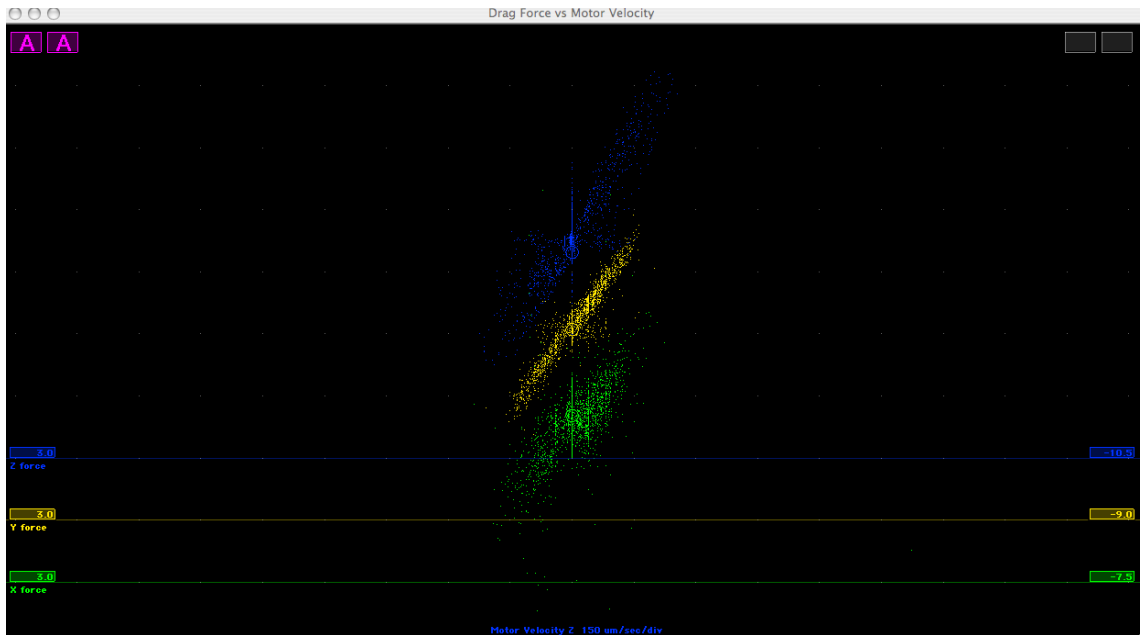
Figure 6. Effective radius of the bead can be extracted from the slope through
Stokes' Law.

nominal size from the bead manufacturer, then all is well. If they do not match well, consider adjusting the calibration factors, namely trapAForceSensitivity[*x,y,z*] and trapBForceSensitivity[*x,y,z*], which may need to be changed.

Cautions: The inter-focal distance, as set by the iris/sum method, will affect the X,Y calibration factors slightly (~10%) but the Z factor will change more. The temperature sensors need to be calibrated (see above) since the water viscosity used in the Stokes' diameter calculation is corrected for ambient temperature. The buffer viscosity must be close to water's. PEG or Glycerol increases the viscosity of buffers greatly. Bead sizes will vary within a batch, so try several beads and average their apparent sizes before accepting or changing a calibration factor. Dirt or long DNA hanging off a bead will increase its drag. It is worth noting that the total force used in the Stokes' law is computed from two detector signals (A and B) multiplied by two sensitivities: trapAforceSensitivity and trapBForceSensitivity. These factors can be assumed to be the same only as long as the optics and detectors are identical. Typical variations in trap sensitivities are on the order of +/-10%, but, unfortunately, the Stokes' test does not tell anything about differences between the two detectors because the force load is not necessarily shared equally between the two beams.

3.2.2: Light Momentum Calibration

Changes in light momentum flux are detected in the Force Sensor Assembly, which comprises of two silicon photodiodes, the PSD detector and the IRIS detector. The dimensions and power sensitivity of these detectors can be used to directly compute the force calibration factors, as mentioned in Optical Tweezers Principles.

The **Raster Test** measures characteristics of both photodiodes as follows:

(1) It tests variation of PSD light sensitivity over its surface area. It detects interference fringes in the optics leading to detectors.

(2) It measures dimensions of the PSD and the magnification of relay lens system.

(3) It tests transmission profiles of Bullseye attenuators.

(4) It checks coincidence of the Bullseye filter's center and PSD detector's center.

The raster test requires an auxiliary diode laser and special mount called the "Raster Test Light Source".

First, remove both objective lenses and their mounting brackets and set them aside. Before starting the test, explore the X-Y motor limits by moving the stage with the mouse and observing the red LED limit indicators on the Motor Control Board. Position the X and Y motors in their Motor Clamps such that they still barely, and lightly, touch the stage when the lead screws are retracted to the limit. Next, adjust the screws until the X and Y motors are near the centers of their ranges. Then, insert the Raster Test Light Source into the motorized stage as though it were a micro-chamber.

The Raster Tester Light Source includes a diode laser which is collimated and masked to give a narrow pencil of light which enters the Prism Box input aperture. To align the beam, the laser needs to be pointed toward the same side as the CCD camera. The angle of the beam should be adjusted with 8-32 Tilt Screws inserted in the chamber holder frame until a spot of light appears near the center of the CCD camera. Next, the Raster Test Light Source beam offset position (not the tilt angle) needs to be adjusted by moving the Chamber Holder Frame up or down in the motorized stage's chamber legs and by turning the clamp screws on the Raster Tester Holster. Use an infrared indicator

tilt screw

diode laser

clamp screw
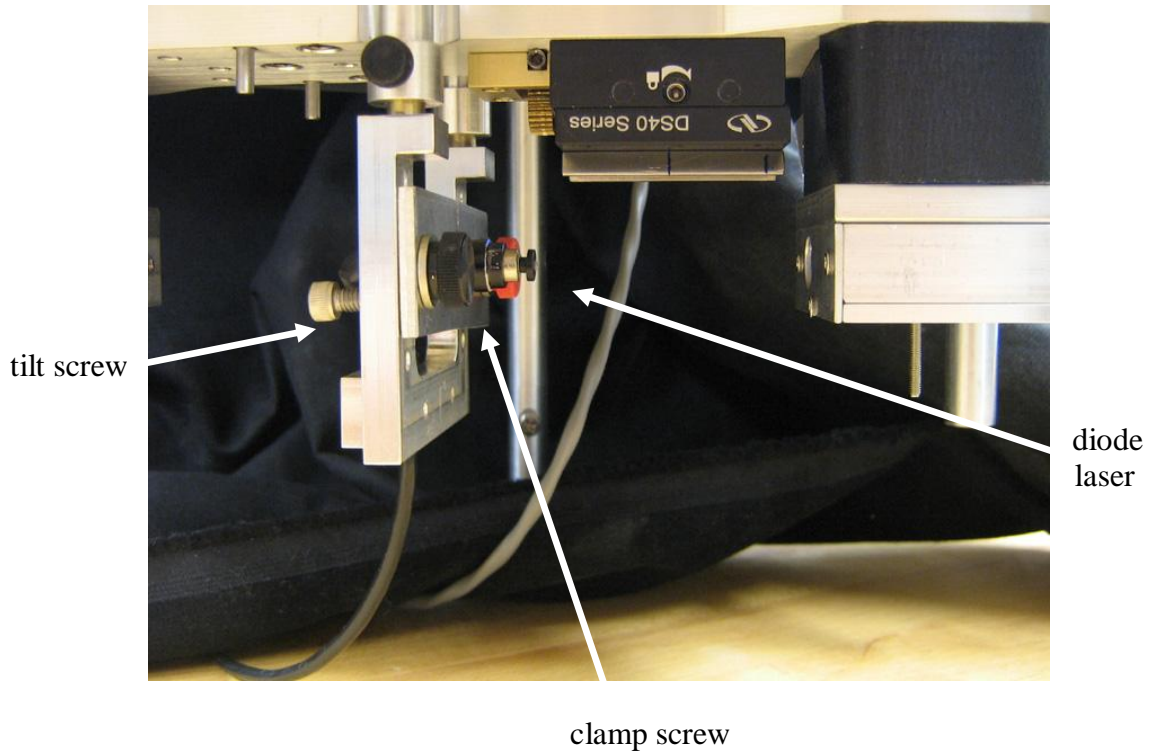
Figure 7. An image of the Raster Tester Light Source is shown installed in place of the microchamber.

card to put the beam near the center of the prism-box aperture. Alternately, it is more accurate to insert an Aperture Iris Button into the aperture and read the PSD Sum in order to place the beam exactly on the center of the prism box aperture. However, be sure to remove the aperture iris button before starting the raster test. Code for controlling the instrument during the raster test scan is shown in the Software section under "Raster Test" at the miniTweezers website (http://tweezerslab.unipr.it). The code provides to the host program functions that cause the motorized stage to move in an X-Y raster pattern covering a 6 mm x 6 mm area. Since the laser beam passes through the plane which would be at the Back Focal Plane (BFP) of the objective lens, and since the X-Y coordinates of that beam at the BFP from the stage motor encoders are known, it is

possible to map the position response of the PSD detector versus the position of any ray in the BFP. It is necessary to record certain channels of data during the raster test, and it is most convenient to have a preference file set aside for such tests. An example PREF file for raster test is given in the Software section of the miniTweezers website under "Raster Test". The host program loads the PREF file when it starts so you would need to replace your usual preference file in your user directory with the Raster Preference file and rename it "PREF". This raster pref file also contains preset locations for the center and 4 extreme corners of the 6mm square pattern. These GOTO locations are numbered 1 through 5. First, be sure to reset the motor PIC (under Tools in host menu) in order to zero the motor positions at the center of the aperture. Stage position #1 (GOTO location 1) will then indicate (0,0,0). Try GOTO positions 2 thru 5 and check the PSD Sum with the laser running at all 4 corner positions. If the sum drops near a zero value, then the beam has fallen outside the aperture at some corner of the raster pattern and therefore the center position (GOTO 1) needs adjustment. If the motor stops before reaching a corner (it should travel +/-3000 µm in X and Y), check the motor's limit lights to see if any are lit. If one is lit, then choose a different part of the motor range for that axis and adjust the light source position screws to compensate so as to keep the beam in the aperture center at motor position #1 = (0,0,0).

Next, open a data file from the host menu bar "Files," or by pressing the "U" key. Then under "Tools," run "Raster X-Y Motor". The raster pattern will take 5-10 minutes to complete. When the motors stop moving, close the data file by pressing "U" a final time. If the motors begin to repeat the same positions, then stop the raster test manually by selecting "Raster X-Y Motor" a second time and close the data file.

3.2.3: Raster Test analysis

To determine PSD dimensions and relay lens magnification, use a plotting program such as Kaleidagraph, Origin, or Excel to import the tab-delimited text from the raster test file. Determine which way the laser was pointing by observing the trapASum and trapBSum columns. Delete columns for the untested side, such as all columns for "B" trap. Create two new "distance" columns by dividing the deflections by the sums. For instance, AdistX = A_PsdX / A_PsdSum and AdistY = A_PsdY / A_PsdSum. Plot the light lever distance AdistX versus Motor_X and AdistY versus Motor_Y. Fit the plots to straight lines and record the slopes. The inverse of the slope is the effective half-width of the PSD in micrometers, assuming the motor position was recorded in the same units. The "effective" width includes the relay lens magnification so that the detector behaves as though it were relocated at the BFP but with a different width than its native width. For the case shown in the figure below, the native half-width of trapB DL-10 detector (r=5 mm) has been magnified to an effective 5.58 mm in X and 5.38 mm in Y, which are given by the inverse of their respective slopes. These effective radii would be used in the light-momentum force calibration equation below as R_{BX} and R_{BY}.
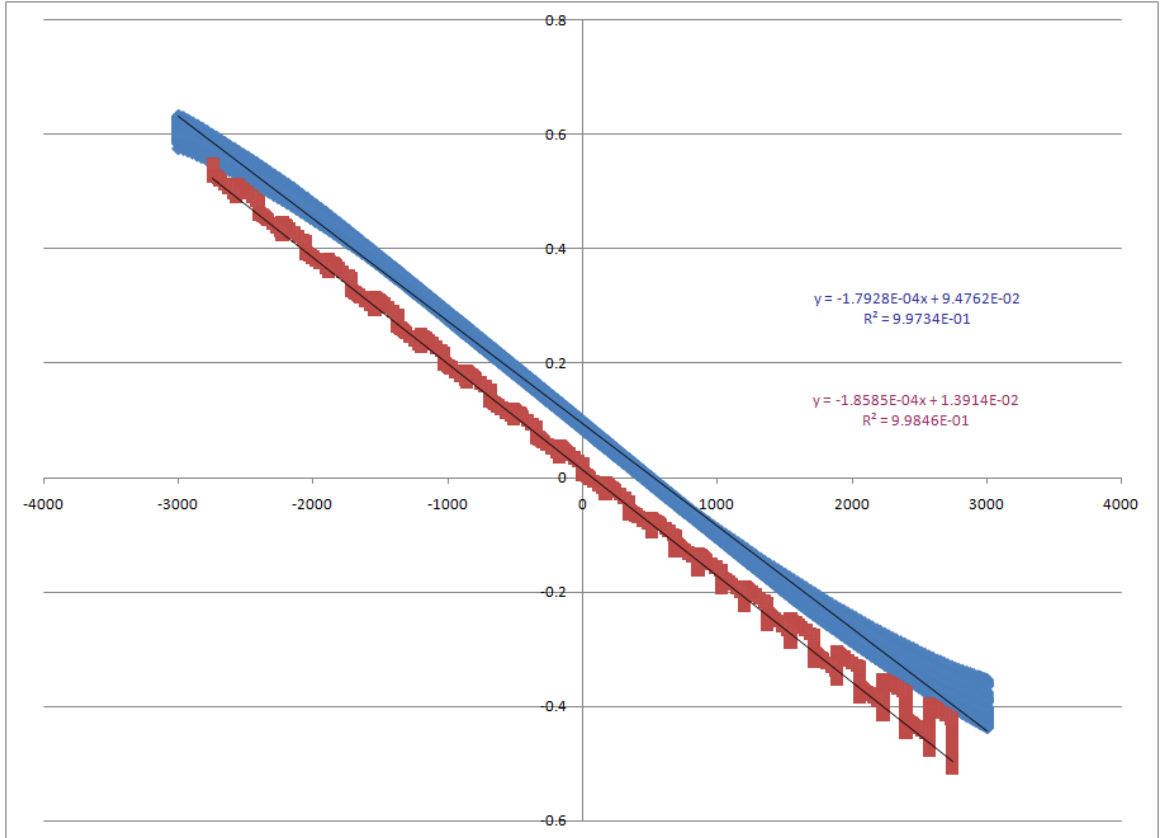
Figure 8. A graph of motor vs. PSD distance is used to calculate the effective radius of the detector.

3.2.4: Power sensitivity test

The PSD preamps give 3 output signals: D_X, D_Y and D_{SUM}

$D_X = \Sigma W_i x_i / R_D$

$D_Y = \Sigma W_i y_i / R_D$

$D_{SUM} = \Sigma W_i$

where the summation is over all rays of light, i, hitting the PSD. Each ray has a power W_i in watts and each ray falling a distance (x_i, y_i) from the center of the PSD which has a half-width R_D. The last equation suggests the power sensitivity can be measured by observing the *SUM* at a known total power hitting the detector. More useful, however, is

the effective power sensitivity, Ψ, which is the ratio of the *SUM* to the power at the trap

focus, assuming all light is collected by the output objective, attenuated by the optics and

projected on the PSD. However, the power at the focus is not directly known, so it must

be inferred from two power-meter measurements by assuming the attenuation in each

objective is identical. To make such an estimate, first install a microchamber, fill it with

water, and add water to the lenses. Turn on both lasers and bring the system to a focus so

that the focal spots can be seen together at the center of the CCD. Nothing should be in

the chamber except clean water. Turn off both lasers and remove the beam blocks

between prism boxes and objectives. Then, turn on one laser and place a thin power-

meter probe between the prism box and objective lens. Take readings on both sides where

the beam goes into the input objective and where it comes out of the output objective (the

back ends of either objective). The power at the trap is the geometric mean of those two

power readings; that is, W_{trap} = sqrt (W_{in} * W_{out}). The effective power sensitivity is given

by $\Psi=SUM / W_{trap}$. Make the measurement for both PSD detectors by running one laser at

a time.

3.2.5: Transverse light force calibration

The Raster Test and Power Sensitivity Test provide values to calibrate light-

momentum forces that are transverse to the optic axis.

F_x = trapAForceSensitivity[x] * D_{XA} + trapBForceSensitivity[x] * D_{XB}

F_y = trapAForceSensitivity[y] * D_{YA} + trapBForceSensitivity[y] * D_{YB}

where (R_L is the focal length of the objective lens, typically 3.00 mm)

trapAForceSensitivity[x]= $R_{\mathrm{AX}}/(c\Psi_{\mathrm{A}}R_L)$ trapAForceSensitivity[y]= $R_{\mathrm{AY}}/(c\Psi_{\mathrm{A}}R_L)$

trapBForceSensitivity[x]= $R_{\mathrm{BX}}/(c\Psi_{\mathrm{B}}R_L)$ trapBForceSensitivity[y]= $R_{\mathrm{BY}}/(c\Psi_{\mathrm{B}}R_L)$

Some problems might be caused by interfering light paths leading from the trap to the PSD detectors, causing sensitivity fringes in the PSD detectors. Small close-spaced fringes are not a problem because the light pattern from the back-focal plane of the trap gets averaged over many such fringes. However, wide fringes, caused by nearly flat windows and prisms, will mean that when the light pattern is deflected to one side (say upward) it hits a high-transmission fringe but when it is deflected in the opposite direction (say downward) it hits a low-transmission region. Thus the calibration sensitivity might be affected by how far the light is deflected (by the force magnitude) and by the direction of that force. Some of the worst fringes occur because the glass window on the front of the PSD makes interference fringes. You can remove the glass window from the PSDs except for those machines which will need to work in a very humid climate, where the silicon might become wet. See "How to remove PSD Glass Cover" under the Documents section of the miniTweezers website to learn about this.

Figure 9. These data were generated by the Raster Test to show Force Detector signals and displayed by the "Raster Test Visualize" program in Software section. The yellow cross indicates the center axes x=0 and y=0. The red/blue stripes indicate +/- 4% variations in intensity.

3.2.6: Longitudinal Light Force

Force acting on the traps in a longitudinal direction (along the optic axis) is detected by the so-called "Iris Detectors". Their outputs are proportional to the concentration of light power near the axis; hence, the cosine projection of the ray powers along the optic axis. These detectors use the Bullseye filter to weigh the rays according to their distance from the axis. The detector outputs are the resulting light power hitting the silicon diode multiplied by the diode sensitivity. The instrument calculates the Z-force by subtracting the two weighted Iris readings as follows:

24

$F_Z = trapAForceSensitivity[z] * Z_A - trapBForceSensitivity[z] * Z_B + nullOffset$

where the nullOffset is measured experimentally for known zero force. The sensitivity

values are given by:

$trapAForceSensitivity[z] = n_{water}/(c\Phi_A)$

$trapBForceSensitivity[z] = n_{water}/(c\Phi_B)$
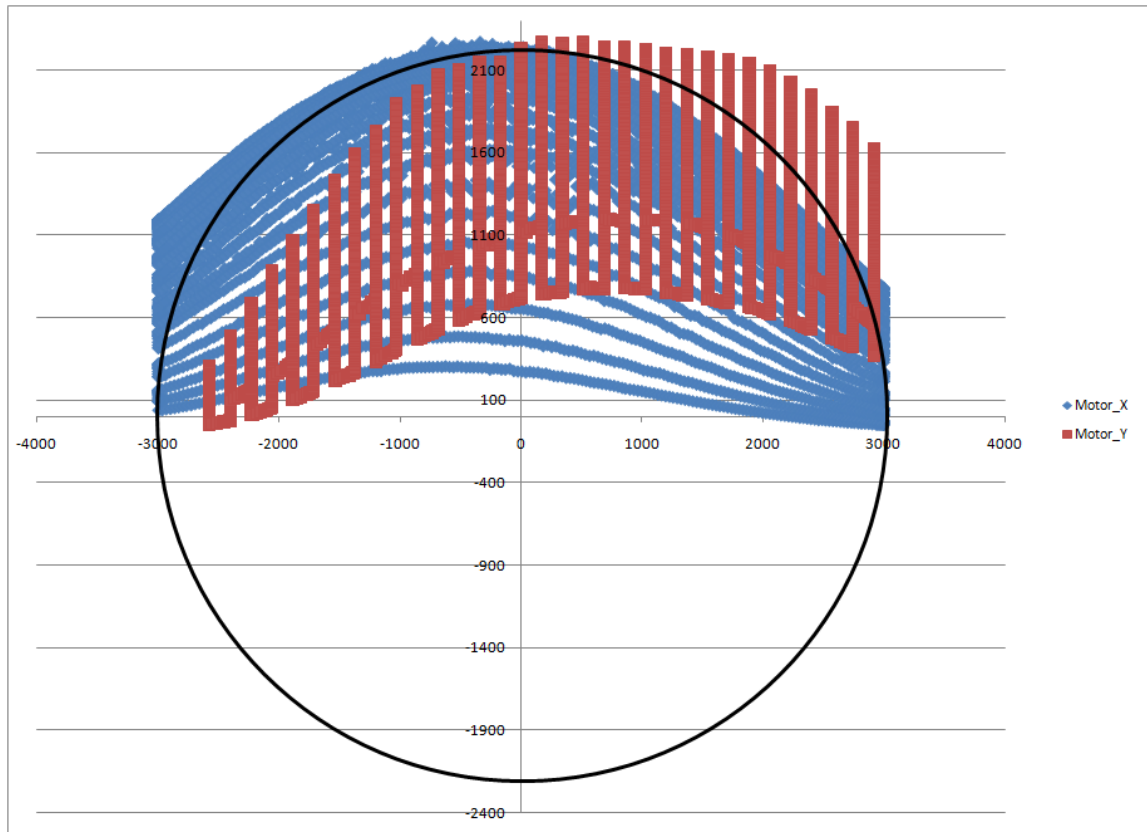
Figure 10. This figure above shows a plot of Iris Detector signal versus X-motor position and Y-motor position for the standard Bullseye filter.

where Φ is the Iris Power Sensitivity = counts/watt from the iris detector. This value is

measured by observing the Iris output for known power at the traps, but the Iris detectors

should have a clear mylar film to simulate a Bullseye with no attenuation except the

Fresnel reflection off the film (~8%). The Iris output may be observed in the Oscilloscope window or else calculated from the PSD SUM multiplied by the Iris/SUM as indicated in the PSD window. The raster test gives a valuable check on the shape of the light transmission of the Bulleye filter. In order to properly score the light momentum flux along the optic axis and derive the Z-axis force, the Bullseye filter needs to have a semi-circular transmission profile with a radius of $n*R_L$ where n is the refractive index of water and f is the objective focal length. For the Olympus 60X objective R_L=3mm and so the Bullseye should have an effective radius (referenced to the BFP) of 4 mm.

Comparing the profile with a circle indicates that the filter has too rapid a variation of transmission with radius. Such a filter gives a signal for the Z-axis force that is too large when using equations shown above for trapAForceSensitivity[z] and trapBForceSensitivity[z].

This next figure below shows a filter which has been adjusted to 45% brightening using an eraser tool set to 45% opacity with 8mm diameter. This brightening will depend on the laser printer. Examples of brightened filters are provided on the same page as the normal Bullseye Filter, 8mm.

The raster test can also be used to check alignment between the centers of the Iris detector bullseye filter and the PSD transverse force detector. Here below is output from the raster-test visualizing program (see Software section) showing the relative position of the Bullseye transmission pattern (red circle) and the PSD neutral positions (deltaX=0
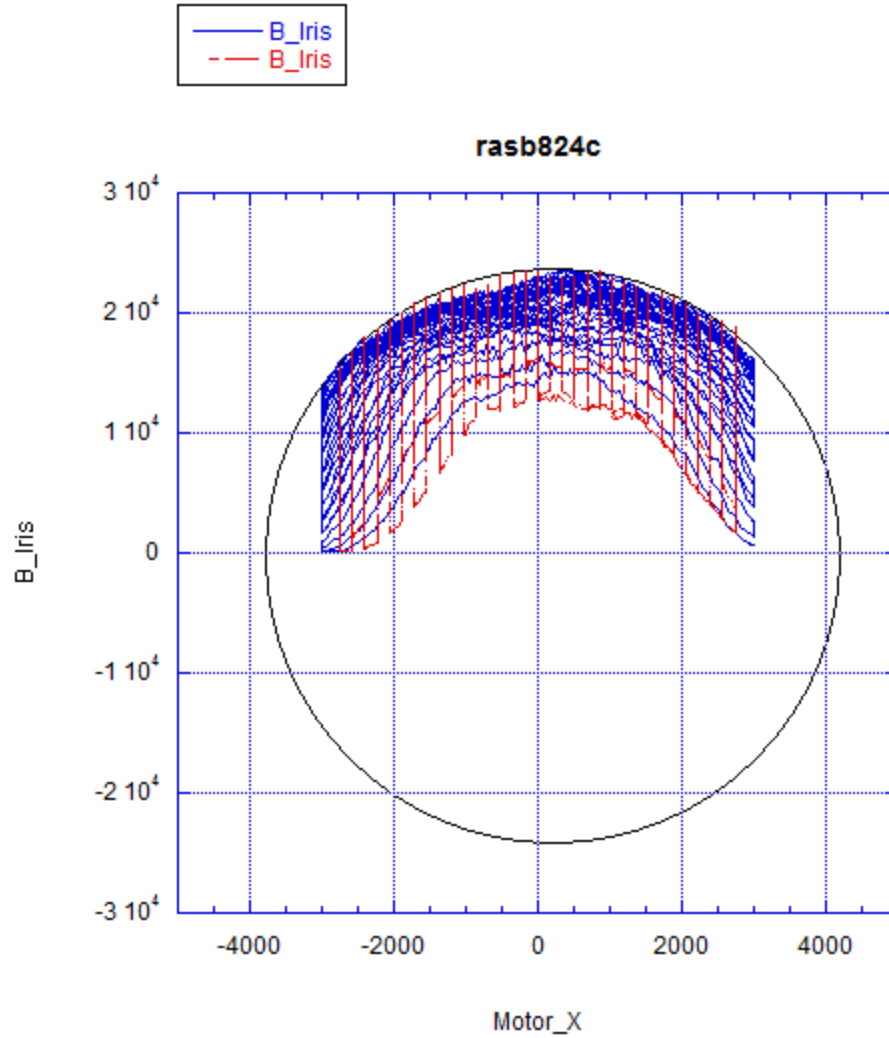
Figure 11. This figure above shows a plot of Iris Detector signal versus X-motor position and Y-motor position for the standard Bullseye filter after corrections made to the Bullseye filter.

and deltaY=0). If the transfer function is not centered, then try adjusting the position of the iris detector circuit board with attached detector and Bullseye filter. To shift the board, remove the flathead screws and replace with round head screws of the same size with washers. Shift the screws in the circuit-board holes and retest until the patterns are centered.
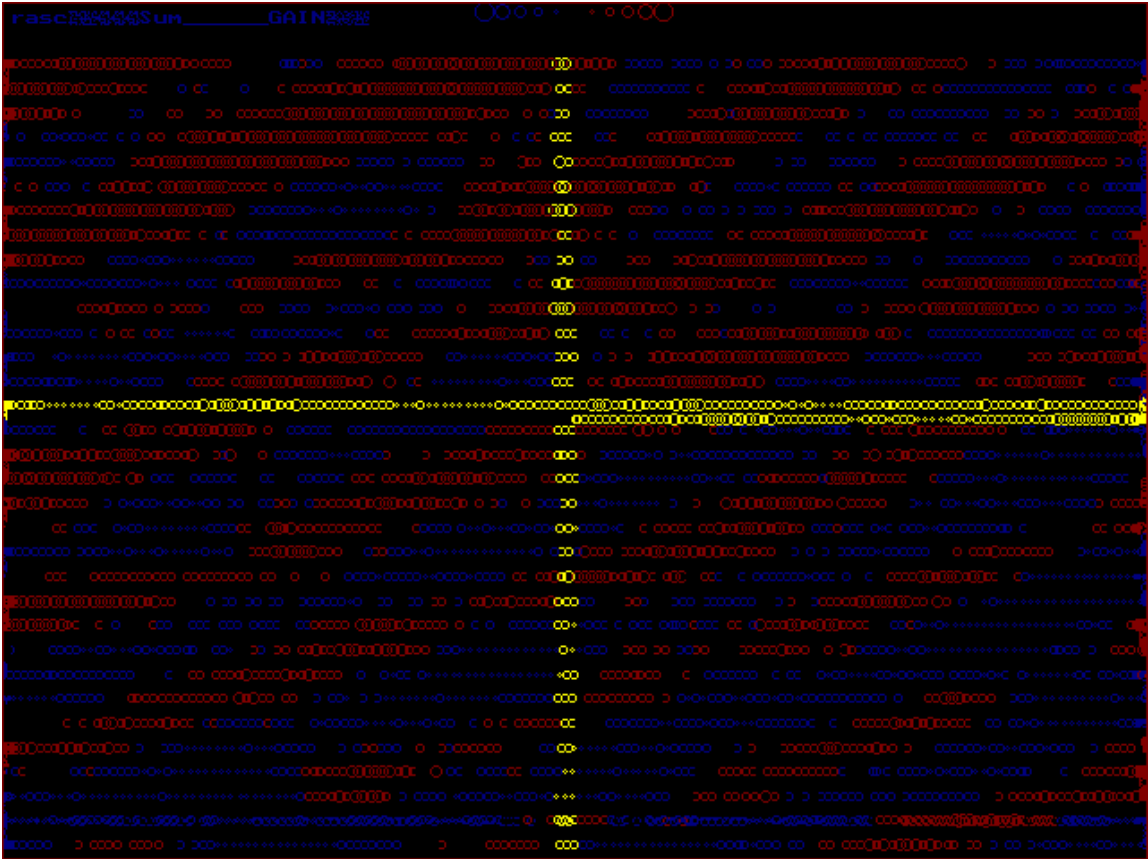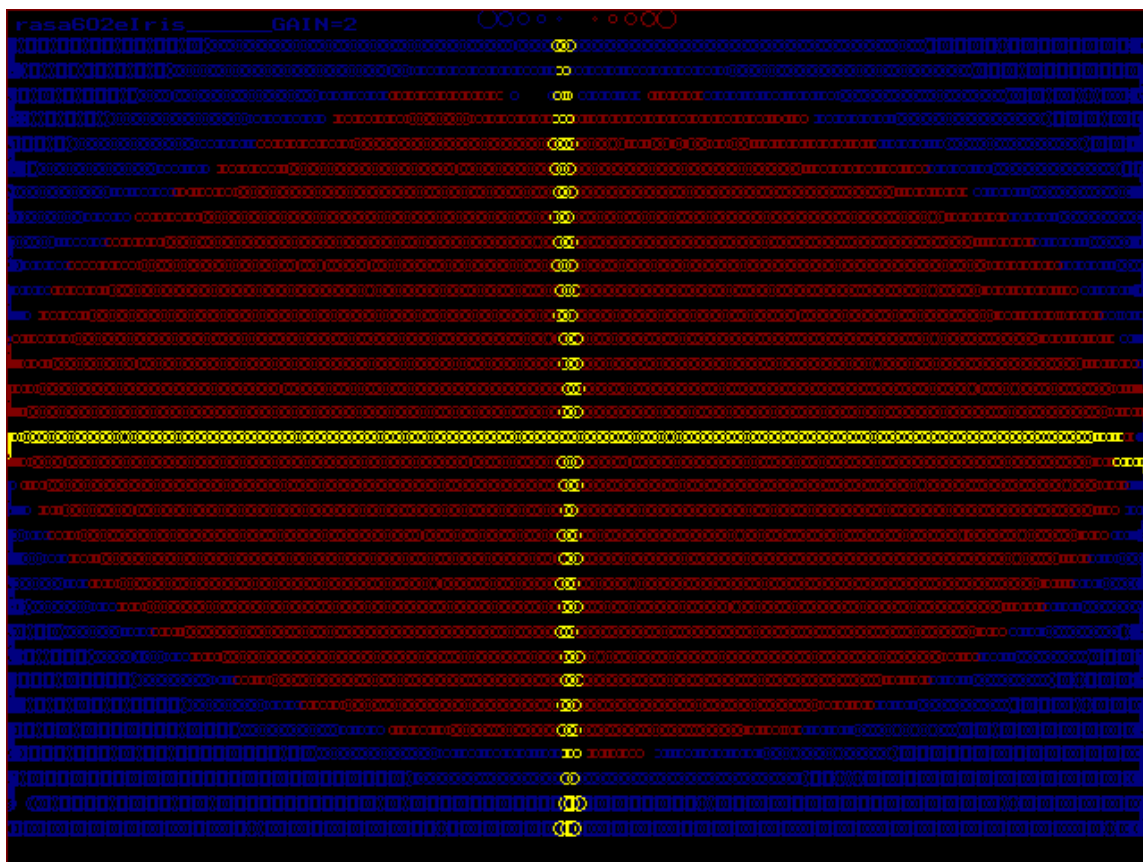
Figure 12. These data were generated by the Raster Test to show Iris signals and displayed by the "Raster Test Visualize" program in Software section. The yellow cross indicates the center axes x=0 and y=0. The red/blue stripes indicate +/- 4% variations in intensity.

3.2.7: Overstretching DNA Force check

A useful test to determine if the force calibration is correct is to measure the overstretching force of dsDNA. To make this test, use a piece of dsDNA with roughly 50% AT base pairs and 50% CG base pairs, such as lambda-phage DNA. Fill the chamber with buffer that has 500 mM NaCl and 10 mM Tris pH 7.5 and 1 mM EDTA. Fish the DNA between 2 beads, one on the pipette and another in the trap. Use a large (3-4 μm) bead in the trap. Pull the molecule and plot stretch response in the Force-Position window. Observe the height of overstretching plateau halfway between the start and end

28

of the plateau. That force should read between 60 and 70 pN. To check for direction

sensitivity in force measurements, pull the same DNA molecule to the right and then left
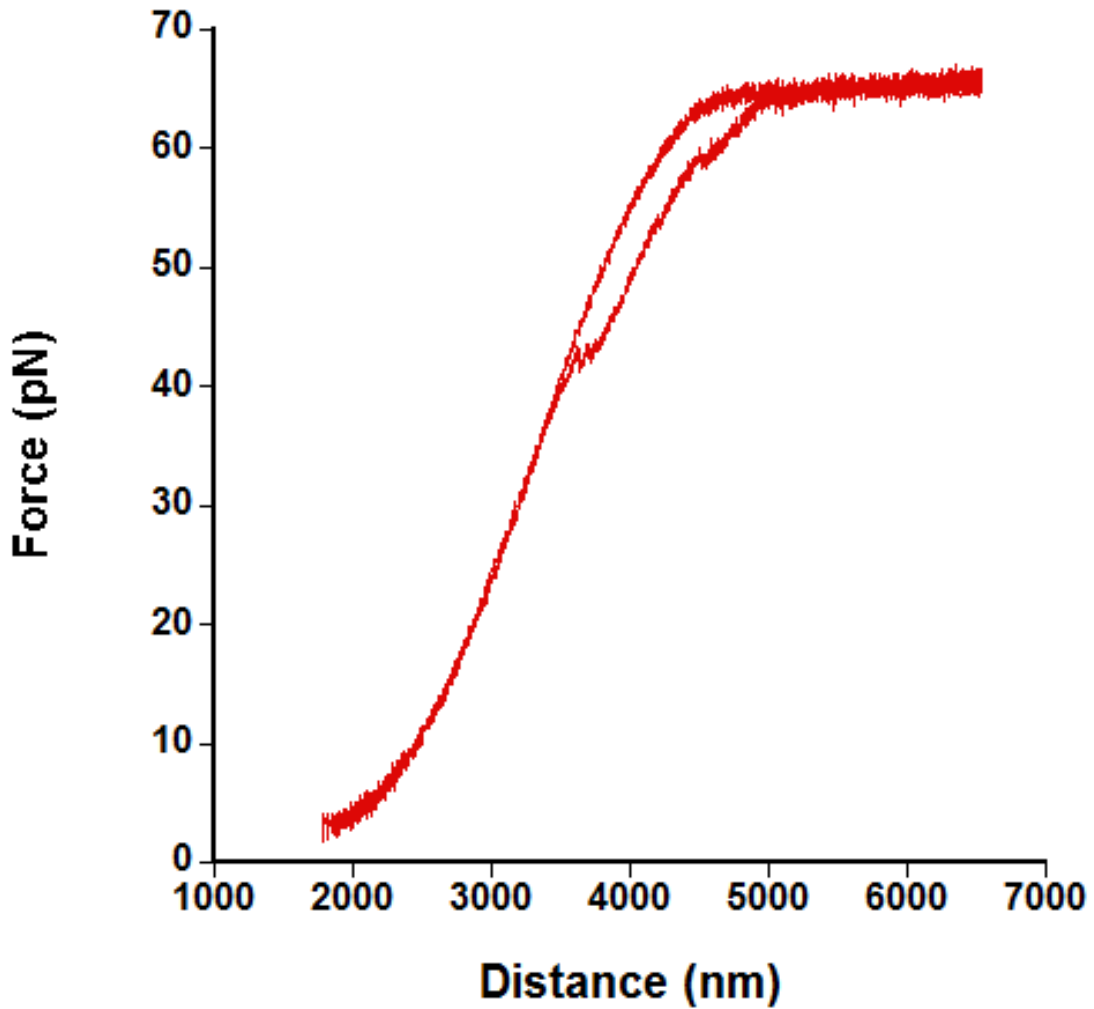
Figure 13. DNA pulling (left to right) and relaxation (right to left) curve showing the overstretching transition at about 65 pN. The melting hysteresis can be seen between 40 to 65 pN.

and then upward or down and compare the measured overstretching forces (see below). It

is best to turn off any autoalign feedback and pull a long molecule like lambda with the

motors, not the piezos. Use autoalign briefly to make the traps coincident before you start

pulling, but turn it off when you pull to high force with the motors. Plot graphs of

MotorX vs. ForceX and also MotorY vs. ForceY and compare forces at the middle of the overstretch transitions.

3.3: Light-Lever Distance Calibration

Light-levers are used to detect changes in trap positions of the two beams. We have an independent light lever for each trap. To calibrate the distance readings requires comparing changes in the normalized light-lever readings (channels = AdistanceX, AdistanceY, BdistanceX, BdistanceY) with changes in the motorized stage shaft encoders (MotorX and MotorY). Here, the trap positions are locked to the motor positions by running constant-force feedback on both traps which are placed inside of a single bead which is sucked onto the end of a pipette. That pipette, in turn, is fixed to the stage and moved a known distance by the motors.

To run the test, install a fluid chamber with a pipette. Center the traps and capture a single bead, between 3 and 4 microns in diameter in both traps. Then, auto-align the traps and zero the force. Next suck that bead onto a pipette and move the pipette to give lowest possible force (under 10 pN). Next, under "Windows" in the menu bar, open the "Motor/Lever" window. Observe the new window and check that the feedback mode is enabled, which shows "F" for both traps (see picture below) and stands for constant-force feedback. Jog the pipette up and down and right and left by pushing the arrow keys. Note that the traps follow the bead over a limited range and patterns develop in the new window as shown in figure below. The response should be fairly linear until the Fiber Wigglers cannot follow the motors beyond beyond their ~10-μm ranges. Always reverse the motor direction when this limit is reached or you will lose the feedback lock.

Hysteresis in the patterns is due to backlash in the motor actuator gears. The slope of the linear regions should be negative one (45 degrees) given that the window has equal length scales per division on the X and Y axes of the graph (vertical scale in nanometers, horizontal in microns). If the straight regions are not at 45 degrees, adjust the calibration factors TrapAleverSensitivity[X,Y,Z] and TrapBleverSensitivity[X,Y,Z] to make the proper slopes. Note the Z-axis sensitivity is always zero (does not matter) because the light levers only measure distances in the X and Y directions. Typical values for both X and Y sensitivities are 8500. Start with those values but check and refine them values with the Motor/Lever window slope test.
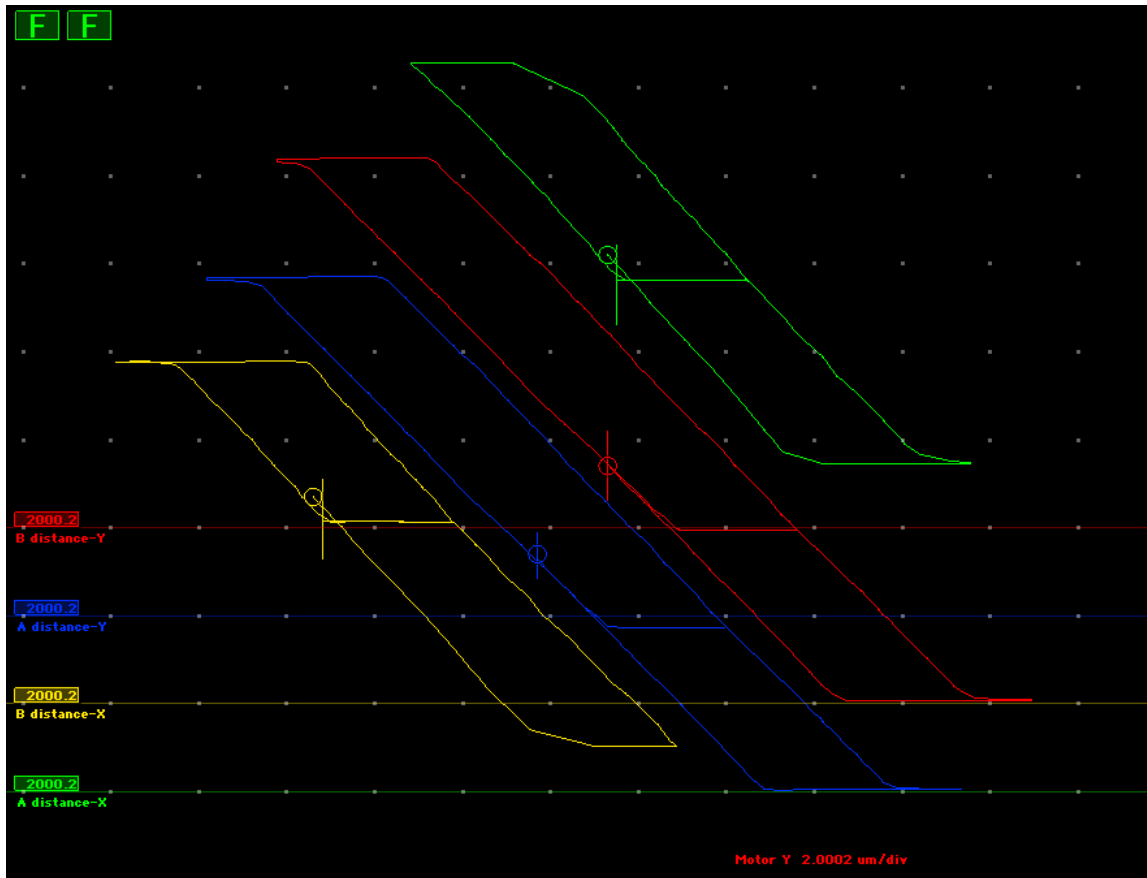
Figure 14. This is a plot of motor distance (X axis) light lever detector distance and light lever detector distance (Y axis). The slopes are tuned to a value of 1 detector unit per nm, so that light lever distance is equal to real distance. The hysteresis seen is due to the motors which use a screw to create motion. A full rotation of the screw is needed before it can move in the opposite direction.

Chapter 4: Optical Tweezers Experimental Protocol

(Step-by-step procedure available for print in the Appendix)

Begin by turning on the power of the Controller Power Supply, Laser Power Supply, and host computer.

Before installing the microchamber, make sure that all the fluidics are correctly applied. Flow in water or buffer through the channels. Check for any leakage at this step because it will tell you if something was poorly connected with the silicone tube adapters. Also, you can look for bubbles that are trapped in the chamber and attempt to remove them. Keep in mind that there are exit-flow tubes which should have their ends placed in the waste vial so that outgoing fluid can be collected. Make certain that there is enough space between the objectives to fit the chamber. The chamber with two size #2 coverslips and two layers of Nescofilm is around 660 μm while the normal spacing between objectives is 880 μm. Insert the chamber carefully, avoiding twists and tilts and touching of the objective lenses. Next, squirt distilled water or an immersion fluid that will not evaporate, like Cargille Labs #43421 (not buffer because it will damage the lenses) between the objectives and chamber so that water displaces all air between the water-immersive lenses.

Run the program named "lt" either from the shortcut on the desktop or the applications bar. (If the bottom windows for PSD, Light Levers, and Force show 0s and the Oscilloscope window shows no changes, then the Main Control Board should be reset. This can be done by pressing the two, white push-buttons on the top board. The button which is closest to the printed "Main Control" words is known as a "hard reset"

because it stops momentarily the signal to the USB port. The other button is a "soft reset" which does the same for the PIC's.

Search for the pipette tip using the Move Motors XYZ button on the host program, "lt." Moving the mouse will cause the motors to move in the X and Y directions. The focus can be changed by moving the motors in and out along the Z-axis. This is done by using the mouse scroll button. Alternatively, motion can also be controlled by one axis at a time by clicking on the corresponding axis button. Finer movement can be controlled by moving 0.1 μm per keystroke using the arrow keys to control X and Y axes or Page Up and Page down for the Z axis. When the pipette tip is found, move away slightly from it, and reset the motor position either by using the tool bar to select Motor -> Zero Motor or by pressing the white push-button on the Motor Control Board (third board from the top). This will allow you to move to the pipette tip location automated by pressing the 1 key. Next, find the position of the dispenser tubes. Each dispenser can be saved to a position, either 2 or 3, by pressing Option+2 or Option+3, respectively. These locations can be saved so that they does not have to be re-saved after restarting the host program by going to File -> Export Preferences (or pressing Shift+U). Old preferences can be retrieved by going to File -> Import preferences.

Protective eyewear suitable for 845 nm laser light should be worn if the laser path is exposed. When the instrument is operating, the six side panels should be attached to the instrument head and the beam blocks should be installed under the prism boxes. The retro-reflector beam block is placed under fiber wiggler A while the plain beam block is

placed under fiber wiggler B. This allows light coming from laser A to be reflected back up into the CCD camera. Check off in the log book that both beam blocks are in place. Turn on the lasers by pressing the red buttons that are labeled "Enable." This will cause the green LED's next to the words "Enabled" to light up. When turning on the lasers for the first time, there are certain parameters to keep in mind. There are five settings which can be chosen to be shown on the LED display. First, is the Laser Current, which is the amount of current being supplied to the laser corresponding to the number of turns using the dials on the bottom. The second is the Power Monitor, which indicates the amount of power exiting the laser at the diode. The third is the Current Limit, which is based on the specifications of each laser. The Power Monitor reading when the laser is at the Current Limit (indicated by the glowing LED next to the word "Limit") should be recorded for future purposes. This value will be referred to as the "Maximum Power Monitor." The fourth setting is the Thermistor Setpoint, which is the resistance value corresponding to room temperature. The lasers will cool until they are close to this value. Consequently, the last setting is the Thermistor Actual, which gives the real temperature of the lasers. If the Maximum Power Monitor is known, then proceed to turn the dials for the two lasers until they are at 50% of the maximum value. Then, look at the CCD TV screen to see the laser spots. It may be necessary to move the Filter Slider in and out to change the type of filter in the path of the CCD camera to one that transmits laser light. The spots should be at the center of the screen, so center the piezos using the Center Traps command in the host program and move them to the center using the Adjustment Rods if necessary. It should be stated that the laser A spot will have a star shape pattern and is moved with the left-hand adjustment rods (and rotatable with the retro prism holder in the

beam block underneath it), while laser B is a single spot which moves with the right-hand adjustment rods. If the laser spot for trap B looks large and diffuse, then this is a sign that there is air somewhere in the optical path between the objectives. Either flow more water through the center channel or squirt more water between objectives and chamber. Additionally, it may be that the correction collar is not set correctly, so make sure that it is at 0.20 for #2 coverslips.

Next, check the Laser Current of both lasers. Choosing the laser which has a lower laser current, turn its dial until its power monitor is at 80% of maximum. The current and power values will be different for each laser diode depending on the built-in laser detector sensitivity. Using the laser with lower current can help prolong the lifetime of the lasers. Then, by looking at the PSD window, turn the dial of the second laser until their PSD SUM is equal to that of the other.

The log book should now have the following values recorded: Power Monitor, Laser Current, PSD SUM, and Iris/Sum (empty trap).

Once again, check that the piezos are in their null position by pressing Center Trap on the host program. If they are offset, then move them back to the center using the X and Y adjustment rods located on the top of the instrument head. Press the "soft reset" button on the Main Control board to remove offsets in the PSD X and Y values. If the X and Y values are greater than 10% of the SUM value, then the relay lenses in the instrument head should be adjusted. Remove the necessary side panels of the head. Loosen the screws holding the relay lens holder, located below the force detector, to move the relay lens by hand until the values are closer to 0 in X and Y. Tighten the screw and reapply the side panels when done. At this point, press the "Zero PSDs" button of the

host program to make X and Y values null their offsets. This step should only be done when there is no bead in the trap.

Prepare beads to be flown into the chamber. Streptavidin-coated (SA) polystyrene beads of 2-µm diameter and 0.5% w/v (~3 pM) concentration are generally used for trapping onto the pipette. Typically, 2 µL will be added to 1 mL of buffer. Then, 15 µL of 4-µm anti-digoxigenin-coated (AD) beads of 0.1% w/v (~0.4 pM) are mixed with an appropriate amount (~4700 antibody sites on a bead) of DNA, proteins, etc. The sample being studied should have a digoxigenin handle to attach to AD beads and a biotin handle to attach to the SA beads. After incubating for 15 minutes, add 1 mL of buffer, and now the beads will be ready for injection.

If this is not the first time that a chamber is being used, a simple cleaning procedure is performed to flush out the three channels of the chamber - top, middle, and bottom. This can be done simply by injecting 1-3 mL of buffer through each channel. The top and bottom channels can inject buffer using a syringe, while the center channel uses an 18 mL vial with arms for connecting a needle tip and for air flow. The center channel tube can be pinched with a clamp on the fluidics tray to change the flow rate in the center channel. After this is done, the chamber should be checked for leaks or bubbles. The beads will be injected into the channels using a syringe connected to tubing that goes to the chamber. This tubing is connected to the chamber by a "silicone tube adapter" which comprises of a short piece of silicone tube that sits firmly inside a hollowed nylon set screw. The screw locks into the chamber frame until there is resistance due to the flat end of the silicone tubing making a seal with the chamber over the entry holes. The longer polyethylene tubing come out of the adapter has outer wall dimensions which make it

lock in the silicone tubing and inner wall dimensions which can hold a needle tip without any leakage.

After removing leaks and bubble, SA beads can be injected into the bottom channel first. Move to the bottom channel dispenser tube by pressing the 2 key in the host program. Depending on the length of the tubing to the chamber, a different amount of bead solution will be necessary until beads can be seen coming out of that tube. For about 50" of #24 tubing, 200 μL is usually sufficient, but more important is to inject slowly so that beads do not flow in too fast into the center channel. You can then trap a bead by moving the motors using the Move Motors XYZ button in the host program. The speed of movement can be changed by sliding the marker in the bar underneath the Move Motors XYZ button. Once a bead is trapped, move it near the pipette tip by pressing the 1 key. Then, move the motors to bring it 1 um above the pipette tip. Withdraw a small amount of beads (few tens of uL) to stop additional SA beads from flowing into the center channel.

Using an empty syringe connected to the needle tip which has tubing going to the micro-pipette, withdraw air to apply negative pressure which should pull the SA bead onto the pipette tip. Capillary forces are usually enough to hold the SA bead on the tip. If there are still some SA beads floating around, loosen the screw on the pinch clamp to the center channel tube which allows more buffer to flow into the center channel. Next, move to the top dispenser channel by pressing the 3 key and begin to inject AD beads.

Chapter 5: DNA Condensation with Histidine-Lysine Polymers

5.1: Motivation

In this study, we applied custom built optical tweezers to study how molecular structural parameters affect decondensation behavior of complex in a direct manner. The single molecule techniques are providing mechanistic insights on biological processes in an unprecedented detail by monitoring the behavior of one molecule at a time[13]. The optical tweezers have been applied to study single chromatin fibers, DNA condensation, and DNA:dendrimer systems previously.[7, 14, 15] Here we investigated the dynamic behaviors of DNA: HK complex to gain insights on how mechanical properties of the nanoplex changes under different environments, which will mimic physiological condition inside the endosome.

Histidine-lysine based peptides are developed as a gene delivery carrier due to its less toxicity and excellent control over their structures.[7, 12, 14, 16] These HK peptides have four branches around a three-lysine core (Fig. 15a). Each branch has a repeating sequence of three histidines and a lysine. We chose two histidine-lysine based peptides, H_3K4b and H_3KG4b to investigate their interactions with DNA.[16-22] For H_3KG4b, two additional glycines are added to each branch at specific locations. Their transfection data show that H_3KG4b is ~10 times more efficient than H_3K4b (Fig. 15b).

This observation is quite surprising based upon small structural differences between the nanoplexes. It clearly implies that the added glycines residues may have a significant impact on the binding and release of DNA, hence affecting transfection efficiency dramatically. To gain further insight on their huge difference in gene delivery

efficiency, we utilized optical tweezers to probe the mechanical properties of DNA:HK peptide complex directly.
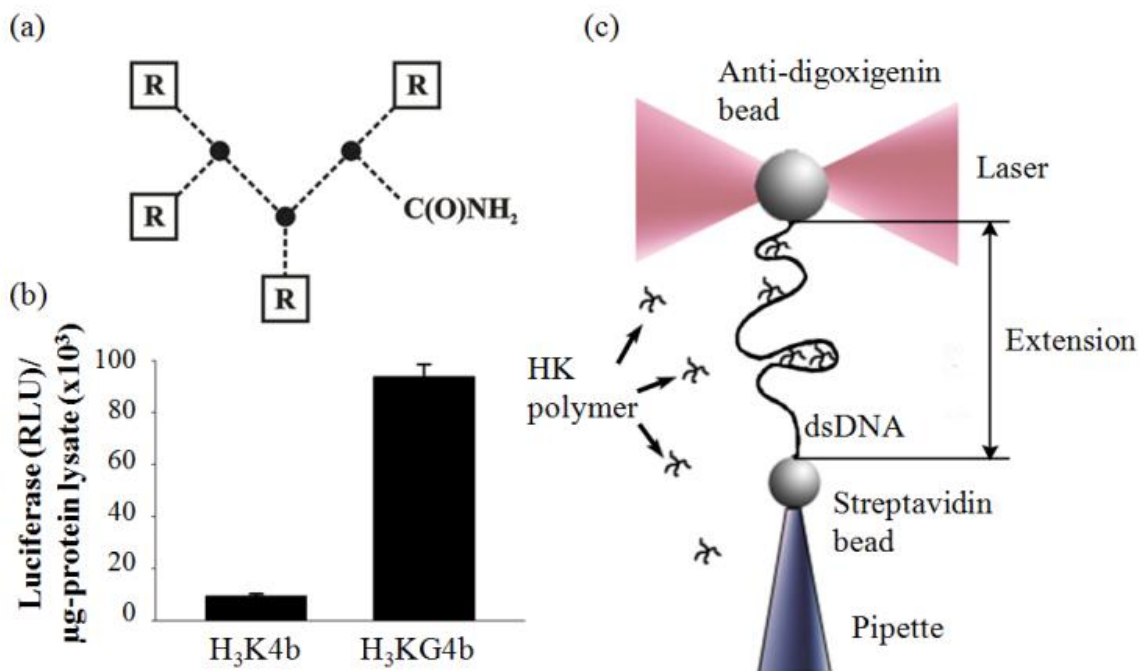
Figure 15. (a) The structure of histidine-lysine based peptide. It has a three-lysine core (black dots) and four branches (R). The branches are connected via isopeptide linkages to the ε-amino group of the lysine. For H_3K4b, R = KHHHKHHHKHHHKHHHK; for H_3KG4b, R = GKHHHKHHHGKHHHKHHHK. (b) Transfection efficiencies of H_3K4b and H_3KG4b. MDA-MB-435 cells were transfected with a luciferase-expressing plasmid. The data represent the mean ± standard deviation of duplicates from 3 experiments. (*$P < 0.001$ in the t-test) (c) A schematic of the experimental setup. A single double stranded DNA (dsDNA) is tethered to each bead through biotin:streptavidin and digoxigenin:anti-digoxigenin antibody interaction, respectievely. As HK peptides are added to the chamber, they condense DNA, causing the extension between the beads to decrease.

5.2: Materials

Experiments are done with two different beads. Streptavidin-coated beads (2.1-μm nominal size, Spherotech, Lake Forest, IL) are trapped on the pipette tip and remain stationary. Anti-digoxegenin beads (4.26-μm nominal size, Spherotech, Lake Forest, IL)

are trapped by the laser tweezers. Double-stranded DNA for the experiments is either 1/2- or 1/3-λ DNA, with biotin and digoxigenin handles on opposite ends. It is made into those shorter fragments from λ-phage DNA (New England Biolabs, Ipswich, MA) using polymer chain reaction (PCR). HK polymers (H3K4b and H3KG4b, Fig. 15a) were synthesized with a Ranin Voyager synthesizer (PTI, Tucson, AZ) in ~30 mg/mL concentrations. The HK polymers were diluted 50 or 100 times in experiments. The buffers used were phosphate-buffered saline (PBS) solution, pH 7.4 and pH 4.2 (modified by adding HCl).

5.3: Experimental Procedure

In our experimental setup, a single DNA molecule is tethered between two beads (Fig. 15c) in a PBS buffer at pH 7.4. One bead is trapped by the laser and the other bead is fixed at the end of the pipette tip. DNA is mechanically stretched to prove that their is a single molecule. When PBS buffer (pH 7.4) containing HK peptide is introduced into a chamber, it condenses DNA into a compact form (Fig. 16) during a constant force clamp of 3 pN. Force clamping will adjust the distance between beads to maintain the set force. If there is an outside force, such as that caused by condensation, it will cause the beads to move closer to each other to return the force to 3 pN. By moving the laser in a constant velocity protocol, this compact DNA:HK peptide complex is stretched and relaxed at 100 nm/sec rate to probe its mechanical properties within a set force range (usually 0-40 pN). Later, the pH 4.2 PBS solution replaces the previous buffer to mimic the conditions inside an endosome. Constant velocity protocol is kept running throughout these two conditions.
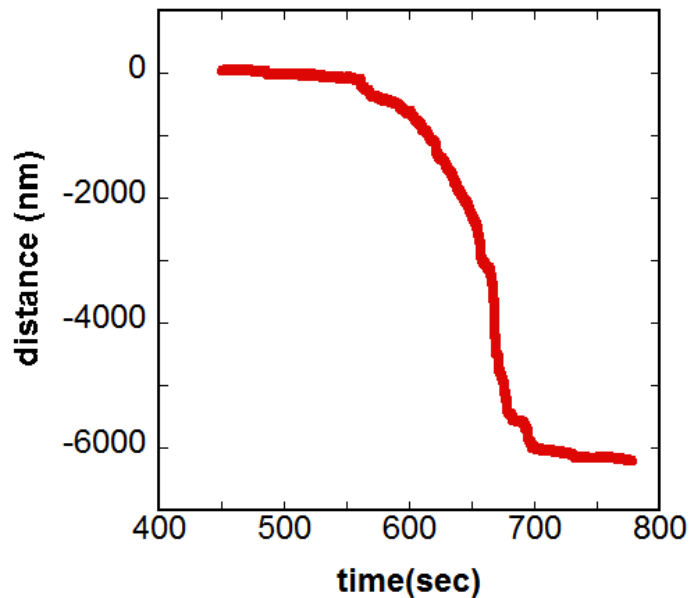
Figure 16. The distance between two beads decreases as the HK polymer is introduced. A constant force mode is used, such that the force caused by DNA condensation causes compaction because the force is maintained at 3 pN.

5.4: Results and Discussion

As the DNA:HK complex is stretched, force increases gradually followed by sawtooth-like features (Fig. 17). During relaxation, the force quickly dropped to below 10 pN and a plateau region was observed around 5 pN with similar sawtooth-like pattern. The relaxation plateau can be explained as the force of reattachment (re-wrapping) of different complex segments, due to lateral contacts arising from the charged HK polymers that are attached to DNA. These are likely due to the intramolecular interactions which are mainly electrostatic. These features with hysteresis between stretching and relaxation curve are repeatable over tens of stretch-relax cycles. The sawtooth-like features indicate the interactions of DNA and HK peptide into a structure that results in unwrapping during stretching and rewrapping during relaxation. This

42
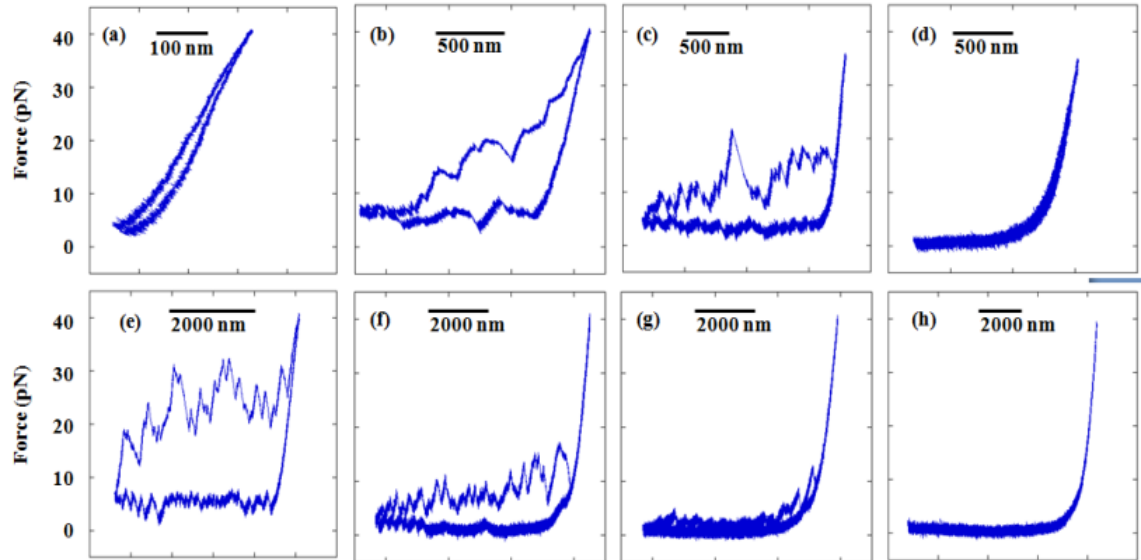
Figure 17. Force vs extension from DNA:HK complex under various salt concentrations. Full contour length of the DNA is 8.4 μm. Curves (a-d) are condensed with H_3K4b at (a) 0.155 M, (b) 0.5 M, (c) 1 M, and (d) 2 M salt concentrations. Curves (e-h) are condensed with H_3KG4b at (e) 0.155 M, (f) 0.5 M, (g) 1 M, and (h) 2 M NaCl concentrations in phosphate buffer.

behavior has been observed in the unfolding of individual nucleosomes in single chromatin fibers.[14] However, single chromatin fibers did not show a relaxation plateau, as observed in our DNA:HK complex. This plateau has been reported in DNA:dendrimer complexes as a result of a phase transition from an extended phase to a condensed phase.[23] Interestingly, the extension during pull/relax cycles was usually significantly shorter than the full contour length of half λ DNA (8.4 μm), indicating that some portion of this complex is not mechanically decondensed in the force range that we used.

To understand the nature of the large hysteresis observed, we examined the effect of salt concentrations. As an ionic strength increased from 0.5 M to 5 M, the amount of the hysteresis was dramatically decreased, indicating that the origin of the hysteresis is mainly electrostatic interaction between DNA and HK peptides.[23] Although we can remove the hysteresis by increasing the salt concentration, the maximum stretching

43

length was still shorter than the contour length. This clearly indicates the presence of two different regions in the complex. There are mechanically decondensible regions and non-decondensible (kinetically-trapped) regions in the DNA:HK complex under varying salt concentrations that we tested. The size of non-decondensible region widely ranges from about 10% to 90% of the total contour length, likely due to kinetics during condensation although it has been difficult to control this consistently. Its length tends to become shorter and disappear when HK concentration was lowered but once it is formed, it tends to maintain its size during the repeated mechanical cycles.

Next, we attempted to mimic the conditions in which DNA:HK complex trapped inside the endosome. The pH inside the endosome can drop as low as ~4, which can significantly influence the properties of the complex. In the case of H_3KG4b, the non-decondensible region was initially over 90% of its contour length (Fig. 19e, blue) but when the solution at pH 4.2 was injected, the non-decondensible region started to expand, reaching at its near full contour length (Fig. 19e, red). The sudden expansion of the complex indicated the drastic change of the mechanical properties in the non-decondensible region at pH 4.2. Once the complex is lengthened, it was stretched out to its near full contour length in the following repeated stretch/relax cycles for an extended period of time (Fig. 19e, green). In the case of H_3K4b, the non- decondensible region at pH 7.4 which was ~60% of its contour length (Fig, 19a, blue) was also immediately expanded to over 90% of its full contour length (Fig. 19a, red) when the pH was lowered to 4.2. However, the non-decondensible region started to
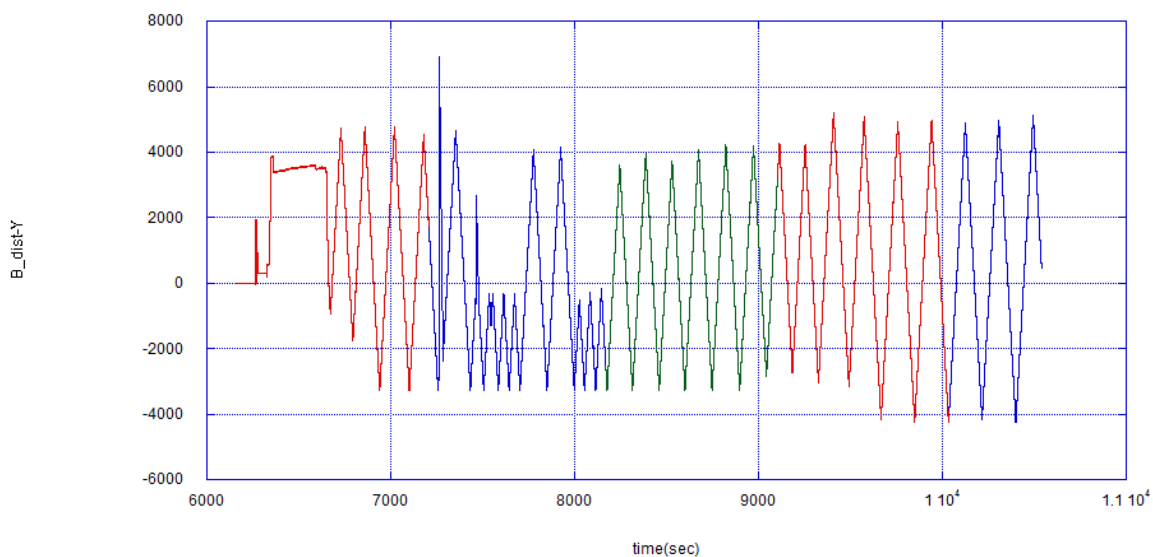
Figure 18. Time versus distance showing the variability in the non-decondensible region for the DNA:H$_3$KG4b complex. The HK polymer was injected at around 6600 secons. The pH is 7.4 until around 8200 seconds, where pH 4.2 solution is injected. The complex loses most of the non-decondensible region at pH 4.2.

reform during the subsequent repeated stretch/pull cycles and it returned to a shorter form (~54%) (Fig 19a, green). This observation is in a sharp contrast with the behavior of H$_3$KG4b where the non-decondensible part at pH 7.4 was extensible once it is lengthened at pH 4.2 for a long period of time.

In some experiments, the expansion at pH 4.2 does not happen immediately, but happens during a future cycle, as shown in Fig. 19. A potential reason for this is that the HK density along the DNA is high enough to cause a net positive charge of the complex. When changing to pH 4.2, the histidines become positively charged, so the structure of the complex is not greatly affected, but there is noticeable decrease in the pulling and relaxation curves (Fig. 19b-c). It is also possible that some of the H$_3$KG4b may be detached at this point, although further evidence is necessary to confirm this. Then, when
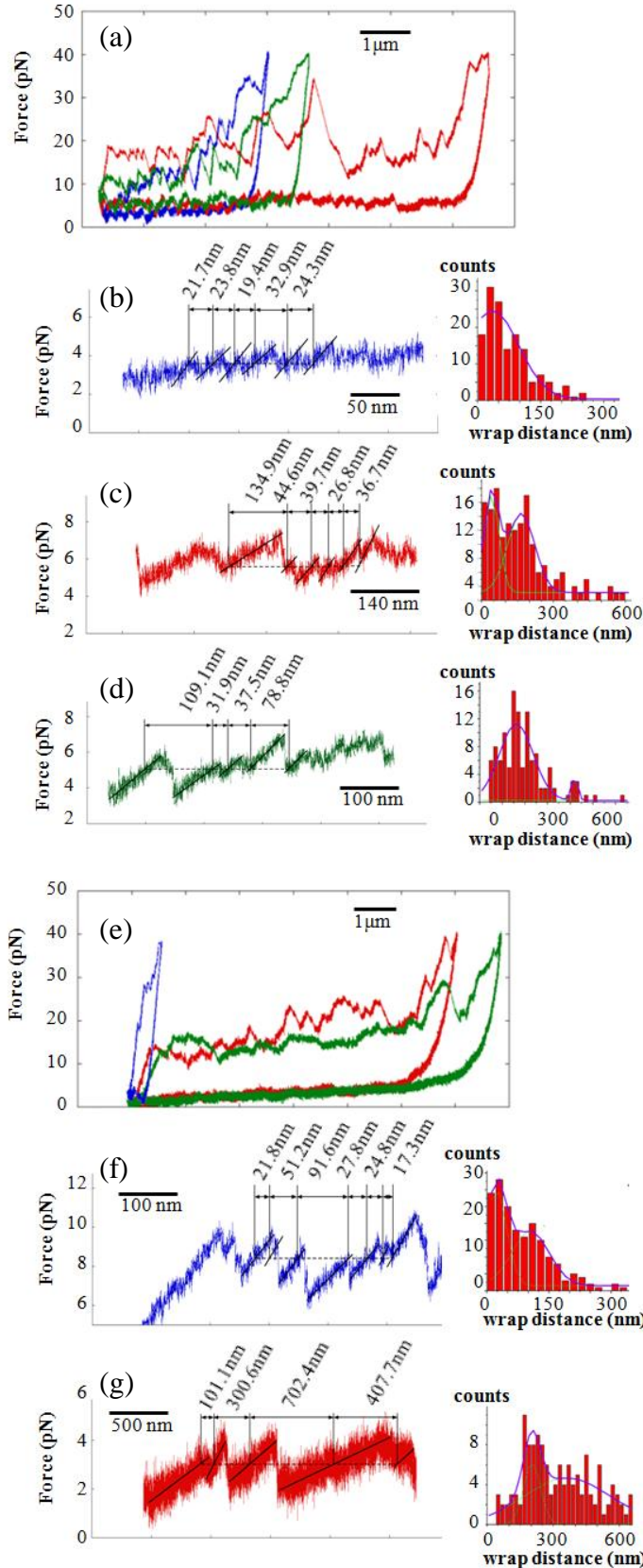
Figure 19. Force-extension curves of the DNA:HK complex at different pH conditions at 155 mM salt concentration. Blue curve is pH 7.4. Red curve is within a minute of introducing pH 4.2 buffer. Green curve is after 30 minutes of initial pH 4.2 introduction. (a-d) are data for H_3K4b, while (e-g) are for H_3KG4b. Histograms represent the wrapping distance between adjacent peaks during the relaxation curves, calculated using a linear fit of the Odijk worm-like chain model. A Gaussian fit was used to calculate multiple peaks using Origin. The major peaks were found to be (b) 35.3 nm ($\pm$ 9.1 nm), (c) 41.7 nm ($\pm$ 6.2 nm) and 165.4 nm ($\pm$ 11.3 nm), (d) 161.7 nm ($\pm$ 8.9 nm), (f) 22.3 nm ($\pm$ 2.5 nm), and (g) 203.5 ($\pm$ 6.0 nm).

the complex returns to pH 7.4, the net charge becomes neutral. Thus, when the pH is lowered to pH 4.2 once more, the complex is able to show the expansion that was seen in previous experiments. Initial charge neutral complex may be a reason why experiments, like in Fig. 16, are able to show expansion during the first pH change.

The expansion at pH 4.2 seen in both HK peptides can be explained by the four-fold increase in the charge density as the histidines become positively charged at low pH. This also results in electrostatic repulsion between neighboring HK peptides, so that the DNA readily expands close to its full contour length. Because of the increase in charge density, there will be an influx of counter-ions to neutralize the sudden charge imbalance. Consequently, the osmotic pressure acting on the endosome wall could potentially result in rupture, serving as the mechanism for release of the DNA from the endosome.

In order to make any claims about how the HK peptide interacts with DNA, we need to think about how the lysine and histidine will bind to DNA. Lysine is positively charged, so it very likely attracts the negative phosphates of DNA, although there is still a chance for lysines to fit between base pairs due to cation-π interactions.[24] Histidine, with its imidazole ring, is uncharged and has a possibility to form π-π interactions (primarily in RNA),[25] or hydrogen-bonding.[24] These two possibilities are the distinction between intercalating and groove binding modes, respectively. To understand which is contributing to interactions between DNA and HK peptide, we need to consider DNA base pairs. In order for there to be π-π interactions, the imidazole ring in histidine would have to stack onto the indole ring of either guanine or adenine.[26] However, hydrogen bonding may be more likely. Both nitrogens in the histidine can interact with the base pairs of DNA through N---H-N (or O---H-N) and N-H---N bonds.[27] There has

47
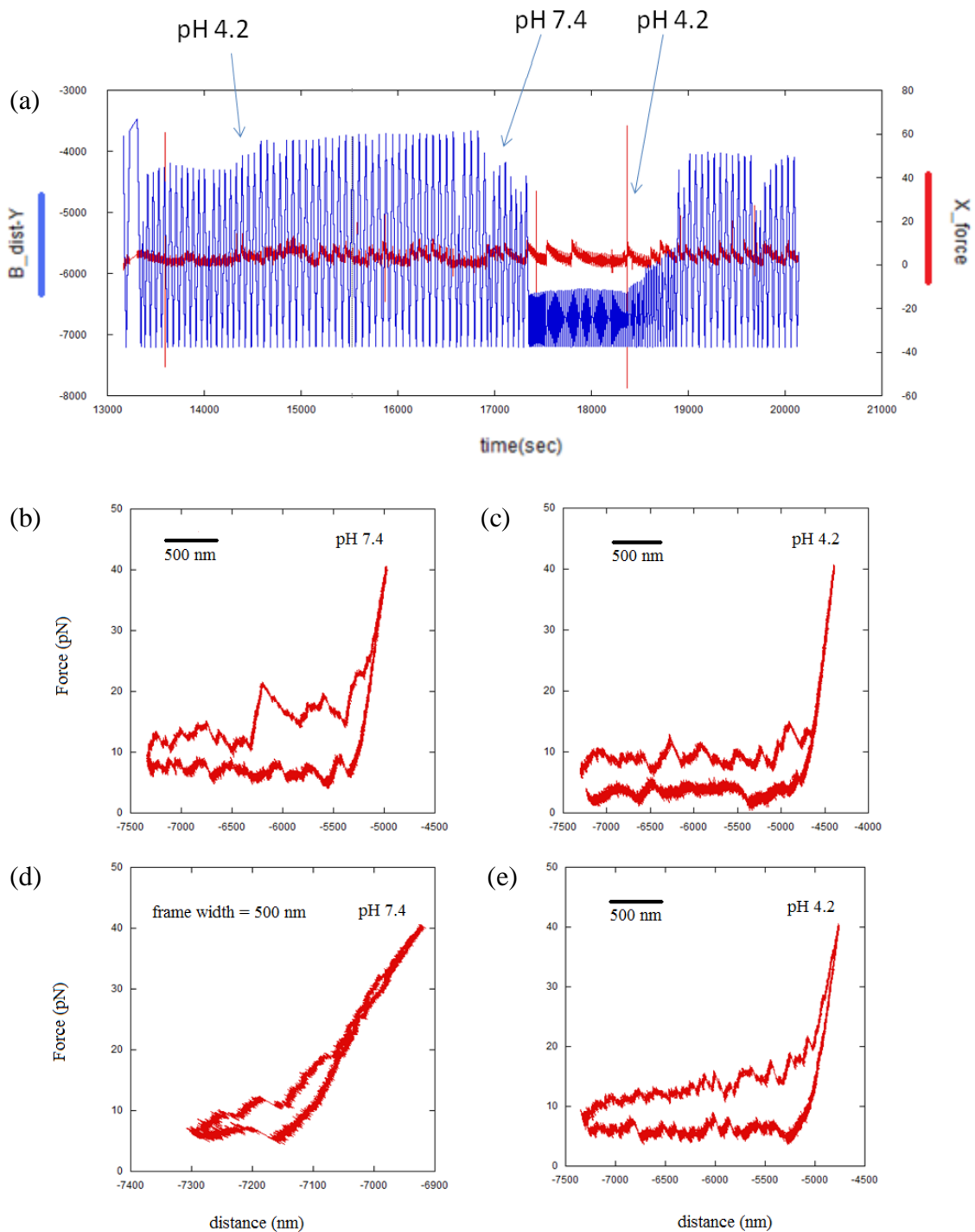
Figure 20. Some experiments (H₃KG4b here) show the expansion at a later cycle. (a) Time points are noted where the pH was changed. Distance is blue and X-force is red. Force data is provided as evidence of injections. (b) Sample curve at first pH 7.4 con-dition. (c) Subsequent change to pH 4.2 shows a decrease in force plateaus. (d) Compaction of the complex seen at pH 7.4. (e) The complex expands at pH 4.2.

been evidence that histidine will interact with DNA, and it was proposed to be due to major grove binding as histidines became protonated.[7] Hydrogen binding has also been suggested by imidazole trimers interacting with DNA through its amines, using NMR.[28, 29]

Because of the combination of lysines and histidines, the HK structures have a mixture of interactions with DNA. This is the reason why salt concentration variation experiments still show that parts of the DNA are still bound to HK peptides, even at 2000 mM NaCl concentration. Although electrostatic interactions seem to disappear as evidenced in the hysteresis, there is another interaction which keeps the HK polymers from completely detaching. Another interesting result is that the hysteresis is very sensitive to a change in salt concentration. The hysteresis decreases as the salt concentration increases, but the DNA is still interacting with HK polymers even at salt concentrations which are large enough to remove hysteresis. The complex has not completely expanded, which means some of the HK remains. It is possible that there are regions of the condensed complex which are weakly decondensing. However, we are not clear yet what drives this strong interaction, but it is sensitive to the protonation of associating and strongly associating. These strongly associating regions withstand the applied force in experiments and prevent histidine at low pH because the complex is able to extend to full contour length in such conditions.

A histogram of the recondensation of DNA around HK peptides shows that the mean length of recondensation, or wrapping, events range between 20-40 nm (Fig. 19b,f), which is comparable in size to chromatin.[29] It is possible for DNA to bend into loop structures as small as 20 nm on its own through "thermal fluctuations,"[30] and the HK

peptide is likely to promote loop closing due to its branched structure. Since the force to condense the fiber is high (3 pN force clamping in experiments corresponds to ~50 bp kinked loops[31]) and the DNA is in saturated concentration of HK peptide, it is expected that loops will be small, as observed in the protein Fis.[29]

When lysines and histidines bind to DNA and form loops, unwrapping is difficult. The DNA:HK complex has only partial decondensation, which is probably due to the combined interaction of lysine electrostatic interactions and histidine groove binding. As a result, portions of the DNA will not decondense (Fig. 19a,d). We believe that the branches of the HK peptides are producing a flexible complex, one which is able to bend as much as or more freely than naked DNA. Using the Odijk Worm-like Chain model, it is possible to calculate the persistence length and stiffness of DNA. This model is give as

$$\frac{x}{L} = 1 - \frac{1}{2}\left(\frac{k_{\mathrm{B}}T}{FA}\right)^{1/2} + \frac{F}{S}$$

where x is the extension, L is the persistence length, T is temperature, F is force, A is persistence length, and S is the stretching modulus. By looking at relaxation curves that had minimal sawtooth features, it is possible to use this model.

It appears that both complexes have lower persistence lengths than naked DNA, with H_3KG4b having a more noticeable change than H_3K4b. Yan and Marko theorized that flexible DNA:protein complexes have strong binding between the DNA and protein,[26] and the same appears in our system. Flexible complexes show an elevated force, which is a common observation with our experimental results. Moreover, the force level increases if the free energy favors the protein-bound state of the complex and the binding strength increases to prevent dissociation of the protein. Indeed, the binding

Table 1. Three curves were used for fitting and then averaged. The standard deviation (in parenthesis) is an average of the errors. "back to pH7.4" means that it was following a cycle from pH 7.4 to 4.2 to 7.4. High salt concentration data was easier to fit due to disappearance of sawtooth features.

Naked DNA

	pH 7.4, 155 mM	pH 4.2, 155 mM	pH 7.4, 5M	pH 4.2, 5M
A	47 (2) nm	29 (1) nm	20 (11) nm	17 (3) nm
S	990 (50) pN	1761 (123) pN	259 (15) pN	350 (19) pN

H₃K4b

	back to pH7.4, 155 mM	pH 7.4, 5M	pH 4.2, 5M
A	44 (17) nm	18 (11) nm	7 (2) nm
S	2500 (limit) pN	703 (151) pN	1072 (52) pN

H₃KG4b

	back to pH7.4, 155 mM	pH 7.4, 5M	pH 4.2, 5M
A	29 (7) nm	12 (2) nm	5 (2) nm
S	133 (10) pN	563 (43) pN	800 (288) pN

strength of HK to DNA can increase the fraction of loops formed even while under tension.[32] This supports our evidence that we cannot dissociate the HK peptide from DNA due to the flexibility of the complex.

At low pH, the histidine becomes protonated. If the histidines are protonated, they repel each other[33] and result in added rigidity[7] for the HK peptide. The resulting four-fold increase in charge reflects an approximately 4- to 9-fold increase in the mean size of wrapping events at low pH (Fig. 19). As the charge becomes more positive, neighboring regions will repel each other. The rigidity is less pronounced in H₃KG4b due to the added flexibility imparted by its glycines. This helps the peptide to "coat" the DNA more effectively and neutralizes charged phosphates on the DNA chain. This is why the

histogram for H_3KG4b displays a second major peak at longer separation distance, due to the difficulty of creating smaller loops. Such a coating behavior has been proposed in a starburst dendrimer peptide system before[14]. Since loops are not easy to form in well-coated regions because of inaccessibility of naked DNA regions being able to interact with an HK branch, the wrapping events occur over longer distances. This improved coating is also why H_3KG4b is able to remain decondensed in a period of over 50 min.

5.5: Conclusions

The structure without glycines, H_3K4b, does not coat the DNA well due to higher rigidity arising from the string of positive charges. Hence, loops may be easier to form, albeit with a larger mean size due to the four-fold increase in charge at lower pH. The decreased ability to coat is why H_3K4b is able to recondense into a shorter form. It has more accessible, naked DNA regions which are able to reconstruct the strong associations which withstand high stretching forces observed at pH 7.4. Also, H_3K4b appears to be more sensitive to the pH change because during its initial decondensation, there are two distinct peaks in the histogram of wrapping distances (Fig. 19c). These two peaks seem to correspond to a mixture of wrapping events observed at pH 7.4 and pH 4.2 (Fig. 19b,d). This is not seen in H_3KG4b (Fig. 19f-g). Since H_3KG4b more rapidly changes its wrapping behavior, this may from the flexibility imparted by the glycine in its structure.

H_3KG4b remains in an expandable form in pH 4.2 which makes the DNA more accessible for expressing the genetic information after it has escaped the endosome and transferred to the nucleus. This provides a direct correlation between the higher transfection efficiency of H_3KG4b and the mechanical behavior of the complex that has

been condensed with this peptide. The added flexibility of the glycines in the structure is conferring properties which allow the condensed complex to remain expanded. The analysis of the recondensation behavior is a future direction we are planning to take to understand the effects of glycine on the structure of H_3KG4b.

The insights from this study will help us to design new HK peptides that interact with DNA optimally, increasing transfection efficiency significantly.

5.6: Future Work

To understand more thoroughly the impact of histidine-lysine peptides on the transfection efficiency of DNA, there are several other experiments which can be done. To probe the importance of histidine, there are three different polymers which can be used to contrast the effects of pH change. Poly-l-lysine and polyethylenimine are both linear chains which have no pH sensitivity at endosomal conditions. They have been used as transfection agents, so it would be imperative to compare their interactions with DNA. Another experiment which we plan to do is with a branched polymer of N_3K4b, similar in structure to H_3K4b but with asparagines instead of histidines. Lastly, we plan to look at the differences between four-branched and eight-branched polymers, since those with eight branches have better transfection efficiency on siRNA, but four-branched polymers are more effective than eight-branched ones[6]. This experiment will require the use of long double-stranded RNA to compare these polymers. We hope to elucidate all these differences by completing the mentioned experiments.

Appendix I: Optical Tweezers Step-by-step Protocol
Last updated: 10/15/2010

1. Turn on power supplies (big switches)
2. Open program: "lt" (desktop; looks like a piece of paper with an A)
   a. If lines/numbers are not fluctuating:
      i. press soft reset and hard reset buttons on top of circuit board
      ii. apple + Q to quit program
      iii. reopen program
3. Suspend optical tweezers using bungee cords
4. Flow in buffer to flush out all three channels
5. Apply **water** between objective lenses
   a. To check to make sure that there's water:
      i. Set laser A to 0, laser B to 40 (Power Monitor Values)
      ii. Pull out filter
      iii. Spot should be small and circular
      iv. Press "Center Trap"
      v. Turn laser A to 40 and align both spots on top of each other in the center
6. Set lasers
   a. Laser A: ~172 (80% of maximum)
   b. Laser B: Adjust current so that (green + yellow) sum is within 10 units of laser A's sum
7. Make sure that trap has no obstructions in it (just water) then hit:
   a. Press "Center Trap"
   b. Check that PSD X and Y are both less than 100 counts
   c. If they are larger than 100, ask for help from an expert user
   d. Press "Zero PSDs"
8. Make sure that light levers are less than 10% of sum
   a. Check with an expert user if they are not
9. Trap SA Bead (location 2: bottom channel)
10. Move bead close to pipet tip (location 1), then retract SA syringe <100 µl
11. Detach syringe from pink needle to trap bead
12. Trap AD Bead (large bead)
    a. Stokes' Test
       i. Move bead away from pipette
       ii. Auto-align
       iii. Top Menu -> Tools -> Stokes' test
       iv. Zero Force
       v. Move motors up/down, left/right, middle scroll – moves the bead in 3D
       vi. Hit F to freeze
       vii. Hit Q or E to tilt graph until it is horizontal
       viii. Press E to check diameter
          1. Average diameter of AD beads is 4.26 microns
       ix. If you don't have a bead in the trap, remember to turn off Auto-align

13. Graph -> Force vs. Position

a. press L for lines
b. press X to adjust axes
c. press Z and Shift + Z to zoom in or out
d. press ; if planning to use constant-force mode
14. Top Menu -> Tools -> P1 to set pulling protocol
a. Example:
    i. Max Force 20 pN
    ii. Min Force 1 pN
    iii. Pull Speed 100 nm/s
    iv. Refold Time 0 s
15. Move AD bead very close to SA bead to attach molecule
a. Change the distance between beads either by using "Move Motors XYZ", using the arrows keys, or using "Move trap" (speed can be adjusted with the bar)
b. Hold within 1 µm distance between the beads for 2 min.
c. Pull back and watch for force increase
d. Use a ruler to measure the length of long DNA
e. Long DNA will begin to show force increase near its contour length
f. Ruler conversion to DNA length: 4mm = 1µm
16. Hit U to start saving
a. Click Documents
b. New Folder, name it YYMMDD
c. Name your file, click save
d. When experiment is done, hit U to stop saving
17. When you Auto-align (When AA appears in top left corner), do these things:
a. Center Trap
b. Zero Force x 2
c. Zero Levers
d. Constant Pos (PP)
18. Press P1 button on the right side to start the pulling protocol
19. After stopping experiment, turn off by:
a. Turn laser dials to 0 and disable lasers
b. Turn off Laser Power Supply
c. Press both reset buttons on the circuit board
d. Turn off the Controller
e. Quit the program

Appendix II: Troubleshooting Protocol

Make sure that all power supplies are turned on and that there is liquid inside the microchamber and water between the objective slides.

Problem: The numbers are not changing in the host program.

1. Press the two reset buttons on the main control board.

2. Turn off the program, and back on.

3. Repeat if necessary.

Problem: No laser spot is visible.

1. Retract the filter using the dongle for the slider. This can be pulled all the way back to show that the lasers are turned on.

2. Click "Center Traps." Confirm that Auto-Align is disabled.

3. Check that there is no bubble by moving the motors.

4. Add water between the objectives (water may evaporate after a few hours).

5. If the problem persists, turn the adjustment robs on the top of the mini-tweezers a full turn left or a full turn right. If there is no spot still, make sure to move back to the original position.

6. If the problem continues, turn the screw (clockwise or counter-clockwise) above the worm gear (brass piece above the objectives) until the laser spot is in focus. The direction of turning correlates to increasing sum signal on the PSD detectors.

Problem: PSD X and/or Y for laser A and/or B are larger than 100.

1. Center the traps and press the soft reset button.

2. Open the side panel where the relay lens is. (Laser B is on the side of the CCD camera, while laser A is on the opposite side.)

3. Loosen the screw for the relay lens.

4. Adjust the position of the relay lens until the values are less than 100 and make sure that the sum value is high (~10,000 at 80% of maximum laser power).

5. Tighten the screw while keeping the value under 100 and place the side panel back on.

Problem: Light lever X and/or Y values for laser A and/or B are larger than 10% of the sum. Or, the light lever sum is small.

1. Center the traps.

2. Adjust the screws of the steering mirror, which are labeled A and B and X and Y.

3. Make sure that the sum value is large (several thousand).

4. If the sum value is small, take turns maximizing the sum signal using screws for either X and Y.

5. Alternate between X and Y until the dot on the host program reaches the center while the sum is large. An indication of correct centering is that the screw turns result in the spot moving up/down or left/right, instead of diagonally.

Problem: Cannot get the bead stuck on the pipette tip.

1. Push on the syringe connected to the pipette tubing until air reaches the tip.

2. Do not retract the syringe, and attempt to trap a bead.

3. If it is still difficult to trap a bead, push on the syringe until a bubble exits the tip.

4. If the bubble does not exit the tip, you need to make a new chamber.

Problem: Beads are not coming out of the dispenser channel.

1. Move the center channel's exit tubing so that the end is below the optical tweezers instrument.

2. Inject more beads into the channel, but be mindful that the speed may be too fast.

3. Move the tubing back to the original position above the fluidics tray and look for beads floating in the center channel.

4. If there are still no beads, block the exit tubing of the channel in question.

5. Apply $1/8^{th}$ turn on the syringe injector screw every 5 seconds for a total of 1 turn.

6. Release the exit tubing and try to inject again.

7. If there are still no beads, inject them through the other channel.

Problem: Cannot trap a bead in the optical trap.

1. Make sure to turn off auto-align or constant-position and center the traps.

2. Check that the spots are on top of each other by retracting the filter using the dongle.

3. Use the adjustment rods on the top of the optical tweezers if necessary. (You must check that the PSD and Light Lever values are still correct.)

4. If you do not see a spot, follow the troubleshooting section "No laser spot is visible."

Problem: Having trouble fishing for DNA between beads.

1. Hold the two beads about 1 μm away from each other for 3 min.

2. Pull back and look for force increase as you extend it.

3. If there is no DNA, try to use the Move Motors XYZ to approach the AD bead from different angle. Move the SA bead along its lower hemisphere.

4. Pull back again, and look for force increase during extension.

5. If this does not solve the problem after several beads, change the SA bead.

6. If this problem persists for a total of 15 beads, consider increasing DNA concentration; using a fresh stock of DNA, AD beads, or SA beads; or increasing incubation time.

Problem: The DNA fiber is too short.

1. There may be multiple DNA strands attached. Try to increase the force to break them off.

2. Contamination may be an issue, so try to trap a new bead. If this problem persists, try preparing new DNA solution.

3. There may have been shearing of DNA during mixing. Do not pipette the DNA solution repeatedly. New DNA solution may be necessary.

Problem: There are small sub-micrometer sized objects floating in the chamber.

1. There is contamination in the microchamber. This requires cleaning of the chamber.

2. Flush out each channel with 1-2 mL of filtered ethanol to remove contaminants.

3. Flush out each channel with 1-2 mL of filtered DI water to remove ethanol.

4. Resume experiment as normal.

Appendix III: RNA Unfolding: Preliminary Data for F1 RNA

As mentioned earlier, this experiment is to find a relationship between results of

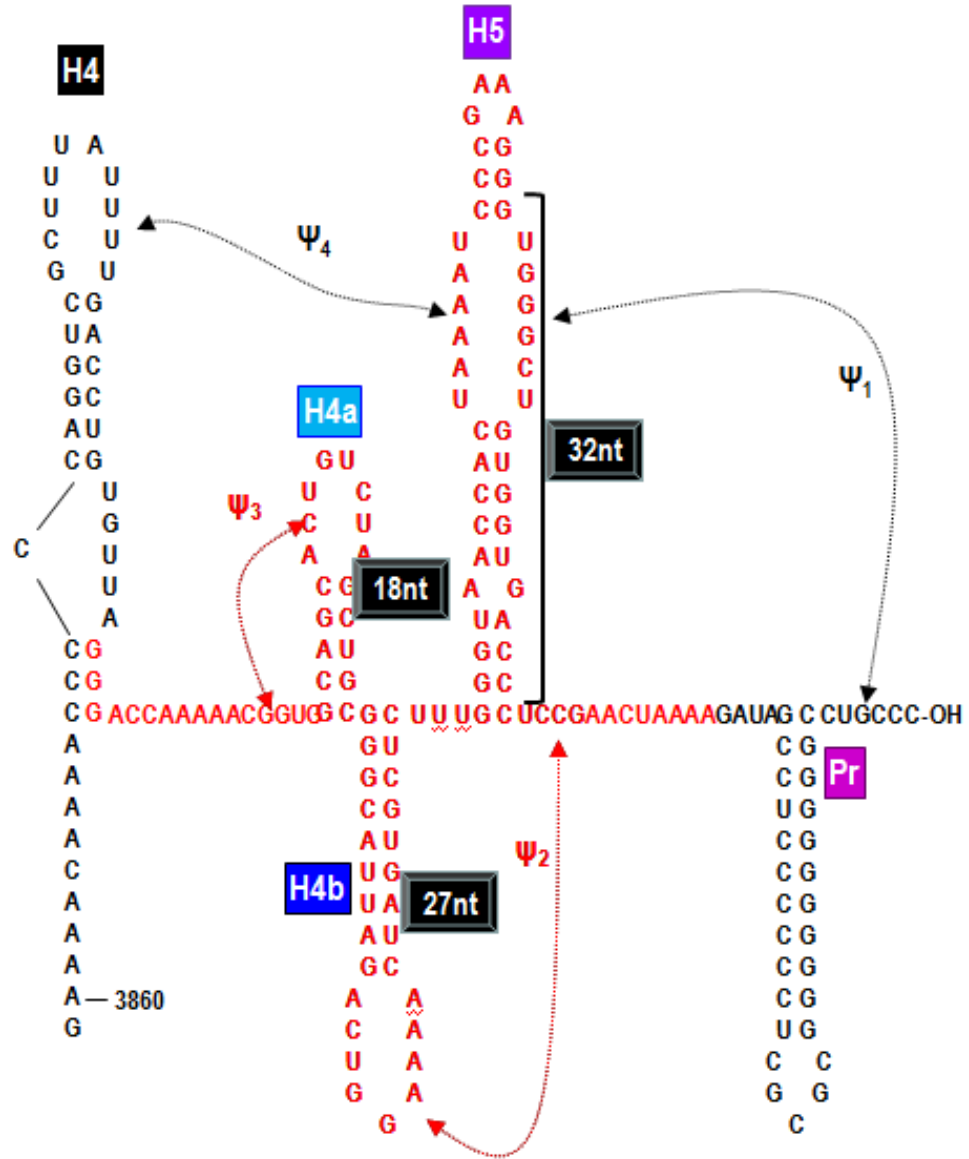unfolding with that of the RNA structure. It should be possible to relate the length of

Figure 21. Shown is the total structure of F4 RNA, but studied is F1 (colored red), which is a total of 99-nt long. H4a, H4b, and H5 are possible hairpins and Ψ_2 and Ψ_3 are psuedoknots.

unfolding regions to a region of RNA, such as the hairpin or pseudoknot. For these experiments we look at a portion of the F4 RNA, which is named F1 (Fig. 21).

RNA experiments are done with or without magnesium, because its presence helps to retain secondary structures, such as pseudoknots. Without magnesium, the pseudoknots would be unstable. By pulling the molecule with optical tweezers, we can observe the different structural elements (Fig. 22). Since the F4 structure is established already, it is possible to relate optical tweezers data with that of the true structure.
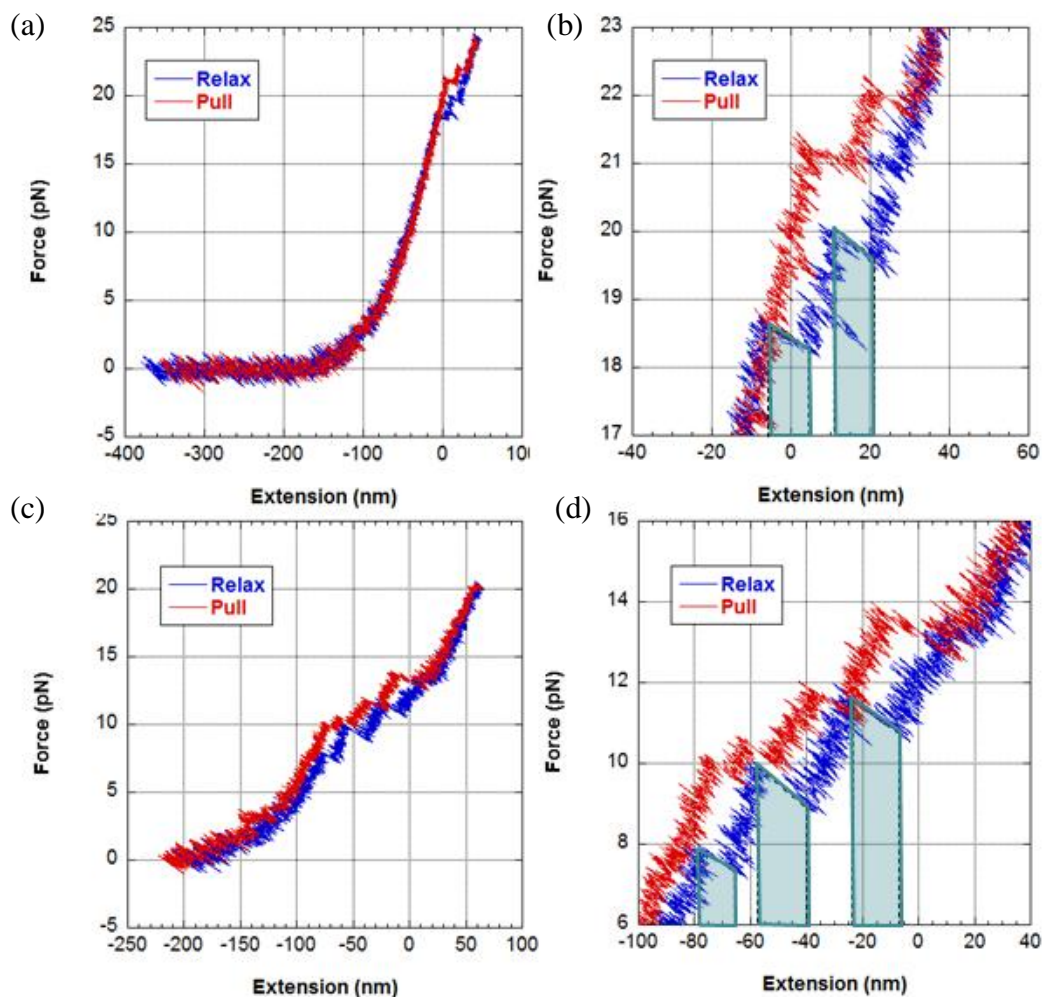

Figure 22. Selected pulling curves for F1 RNA without magnesium. Unfolding has been seen both at high forces (a-b) and lower forces (c-d). The area colored in blue relates to the energy of unfolding of the RNA structural element.

61

Currently, more data is being collected to find the distribution of unfolding events. A histogram of the unfolding lengths should correspond to the lengths of the hairpins. Next, the RNA can be probed in the presence of magnesium. Since the hairpins have been sorted, the other secondary structures can be pinpointed separately. By showing that optical tweezers can give information about the hairpins and pseudoknots, we have evidence that it can find the lengths of hairpins of an unknown RNA structure, which has uses in cataloguing new viruses.

Bibliography

1. Bonetta, L., *The inside scoop-evaluating gene delivery methods.* Nature Methods, 2005. **2**(11): p. 875-+.

2. Tecle, M., M. Preuss, and A.D. Miller, *Kinetic study of DNA condensation by cationic peptides used in nonviral gene therapy: Analogy of DNA condensation to protein folding.* Biochemistry, 2003. **42**(35): p. 10343-10347.

3. Wagner, E., et al., *Influenza-Virus Hemagglutinin-Ha-2 N-Terminal Fusogenic Peptides Augment Gene-Transfer by Transferrin Polylysine DNA Complexes - toward a Synthetic Virus-Like Gene-Transfer Vehicle.* Proceedings of the National Academy of Sciences of the United States of America, 1992. **89**(17): p. 7934-7938.

4. Swami, A., et al., *Imidazolyl-PEI modified nanoparticles for enhanced gene delivery.* International Journal of Pharmaceutics, 2007. **335**(1-2): p. 180-192.

5. Pichon, C., C. Goncalves, and P. Midoux, *Histidine-rich peptides and polymers for nucleic acids delivery.* Adv Drug Deliv Rev, 2001. **53**(1): p. 75-94.

6. Leng, Q.X., et al., *Histidine-lysine peptides as carriers of nucleic acids.* Drug News & Perspectives, 2007. **20**(2): p. 77-86.

7. Bennink, M.L., et al., *Unfolding individual nucleosomes by stretching single chromatin fibers with optical tweezers.* Nature Structural Biology, 2001. **8**(7): p. 606-610.

8. Chen, G., J.D. Wen, and I. Tinoco, Jr., *Single-molecule mechanical unfolding and folding of a pseudoknot in human telomerase RNA.* RNA, 2007. **13**(12): p. 2175-88.

9. Green, L., et al., *Characterization of the mechanical unfolding of RNA pseudoknots.* J Mol Biol, 2008. **375**(2): p. 511-28.

10. Li, P.T., C. Bustamante, and I. Tinoco, Jr., *Unusual mechanical stability of a minimal RNA kissing complex.* Proc Natl Acad Sci U S A, 2006. **103**(43): p. 15847-52.

11. Wen, J.D., et al., *Force unfolding kinetics of RNA using optical tweezers. I. Effects of experimental variables on measured results.* Biophys J, 2007. **92**(9): p. 2996-3009.

12. Smith, S.B., Y.J. Cui, and C. Bustamante, *Optical-trap force transducer that operates by direct measurement of light momentum.* Methods Enzymol, 2003. **361**: p. 134-162.

13. Mehta, A.D., K.A. Pullen, and J.A. Spudich, *Single molecule biochemistry using optical tweezers.* FEBS Lett, 1998. **430**(1-2): p. 23-7.

14. Ritort, F., et al., *Condensation transition in DNA-polyaminoamide dendrimer fibers studied using optical tweezers.* Physical Review Letters, 2006. **96**(11): p. -.

15. Baumann, C.G., et al., *Stretching of single collapsed DNA molecules.* Biophysical Journal, 2000. **78**(4): p. 1965-1978.

16. Wang, M.D., et al., *Stretching DNA with optical tweezers.* Biophysical Journal, 1997. **72**(3): p. 1335-1346.

17.   Ashkin, A., *Acceleration and Trapping of Particles by Radiation Pressure.* Physical Review Letters, 1970. **24**(4): p. 156-&.

18.   Grier, D.G., *A revolution in optical manipulation.* Nature, 2003. **424**(6950): p. 810-816.

19.   Neuman, K.C., et al., *Ubiquitous transcriptional pausing is independent of RNA polymerase backtracking.* Cell, 2003. **115**(4): p. 437-447.

20.   Hansen, P.M., et al., *Expanding the optical trapping range of gold nanoparticles.* Nano Letters, 2005. **5**(10): p. 1937-1942.

21.   Kellermayer, M.S.Z., et al., *Elastic properties of the titin molecule measured using an optical trap.* Biophysical Journal, 1997. **72**(2): p. Mama7-Mama7.

22.   Svoboda, K. and S.M. Block, *Optical Trapping of Metallic Rayleigh Particles.* Optics Letters, 1994. **19**(13): p. 930-932.

23.   Auweter, S.D., F.C. Oberstrass, and F.H.T. Allain, *Sequence-specific binding of single-stranded RNA: is there a code for recognition?* Nucleic Acids Research, 2006. **34**(17): p. 4943-4959.

24.   Cheng, A.C., et al., *Recognition of nucleic acid bases and base-pairs by hydrogen bonding to amino acid side-chains.* Journal of Molecular Biology, 2003. **327**(4): p. 781-796.

25.   Shiraki, K., et al., *Contribution of an imidazole-indole stack to high catalytic potency of a lysine-specific serine protease, Achromobacter protease I.* Journal of Biochemistry, 2002. **131**(2): p. 213-218.

26.   Burckhardt, G., C. Zimmer, and G. Luck, *Conformation and Reactivity of DNA in Complex with Proteins .3. Helix-Coil Transition and Conformational Studies of Model Complexes of Dnas with Poly-L-Histidine(+).* Nucleic Acids Research, 1976. **3**(3): p. 537-559.

27.   Yang, X.L., et al., *Imidazole-imidazole pair as a minor groove recognition motif for T : G mismatched base pairs.* Nucleic Acids Research, 1999. **27**(21): p. 4183-4190.

28.   Wiggins, P.A., et al., *High flexibility of DNA on short length scales probed by atomic force microscopy.* Nature Nanotechnology, 2006. **1**(2): p. 137-141.

29.   Sankararaman, S. and J.F. Marko, *Formation of loops in DNA under tension.* Physical Review E, 2005. **71**(2): p. -.

30.   Skoko, D., et al., *Low-force DNA condensation and discontinuous high-force decondensation reveal a loop-stabilizing function of the protein Fis.* Phys Rev Lett, 2005. **95**(20): p. 208101.

31.   Yan, J. and J.F. Marko, *Effects of DNA-distorting proteins on DNA elastic response (vol E 68, art no 011905, 2003).* Physical Review E, 2003. **68**(3): p. -.

32.   Podgornik, R., P.L. Hansen, and V.A. Parsegian, *Elastic moduli renormalization in self-interacting stretchable polyelectrolytes.* Journal of Chemical Physics, 2000. **113**(20): p. 9343-9350.

33.   Chen, W., N.J. Turro, and D.A. Tomalia, *Using ethidium bromide to probe the interactions between DNA and dendrimers.* Langmuir, 2000. **16**(1): p. 15-19.